ANVIL EFFECT IN SPHERICAL INDENTATION TESTING ON SHEET METAL

A Thesis

by

MAYURESH MUKUND DHAIGUDE

Submitted to the Office of Graduate Studies of
Texas A&M University
in partial fulfillment of the requirements for the degree of

MASTER OF SCIENCE

August 2006

Major Subject: Mechanical Engineering

ANVIL EFFECT IN SPHERICAL INDENTATION TESTING ON SHEET METAL

A Thesis

by

MAYURESH MUKUND DHAIGUDE

Submitted to the Office of Graduate Studies of
Texas A&M University
in partial fulfillment of the requirements for the degree of

MASTER OF SCIENCE

Approved by:

Chair of Committee,	Jyhwen Wang
Committee Members,	Steve Suh
	Angie Hill Price
Head of Department,	Dennis L. O'Neal

August 2006

Major Subject: Mechanical Engineering

ABSTRACT

Anvil Effect in Spherical Indentation Testing

on Sheet Metal. (August 2006)

Mayuresh Mukund Dhaigude, B. Eng., University of Pune, India

Chair of Advisory Committee: Dr. Jyhwen Wang

A spherical indentation test is considered to be invalid if there is presence of a visible mark on the side of the sheet metal facing the anvil and exactly below the indentation. With the available standard loads of the conventional testers such as Brinell and Rockwell hardness testers, it is difficult to avoid this anvil effect while dealing with the sheet metals.

The penetration depth increases when the thickness of the sheet is reduced at constant indentation pressures. The reason behind this is the change in mode of deformation. When the thickness of the sheet metal is reduced, and the indentation test is carried out on it, then the sheet metal experiences first indentation, then bending, followed by lifting of the sheet from the anvil which leads to a forging mode of deformation. The modes of deformation were identified using a finite element simulation of the indentation process. Plots of normalized depth against normalized thickness were created for the same indentation pressure, and a second order polynomial curve was fitted to the data points.

The equation of this curve quantifies the anvil effect. The anvil effect was identified as a function of sheet thickness, indenter radius, indentation load and two material constants. A method to correct this anvil effect was also developed using the equation representing the anvil effect. It is possible to obtain the equivalent geometry of indentation without anvil effect. A MATLAB program is developed to obtain the parameters defining the curve for the anvil effect. Indentation test on a sheet using three different indenters and corresponding loads is required for this method. For accurate prediction of the equivalent depth of indentation, a lower limit of 10 % and upper limit of 80 % for penetration depth (ratio of depth of indentation and thickness of sheet metal) was identified for the spherical indentation testing on the sheet metals. Verification of the curve fitting model was carried out with the indentation experiments on commercially available Niobium, Al2024-T3, Al7075-T6 and 1020 low carbon steel sheets. These tests show good agreement between fit, prediction, and experiments for the anvil effect.

To my loving parents and brother

ACKNOWLEDGMENTS

I would like to take this opportunity to express my honest gratitude to my advisor, Dr. Jyhwen Wang for encouraging me through out the graduate studies and guiding me to perform better. Discussions with him always inspired me. I appreciate him spending his precious time and sharing knowledge which motivated me to think creatively.

I would also like to extend my gratitude to Dr. Steve Suh for motivating me and helping me in taking important decision in my graduate life. My sincere thanks to Dr. Angie Hill Price for serving as my advisory committee member and for all the cooperation she has rendered. Her knowledge in metallurgy helped me a lot in the final stages of my research. I also appreciate her help and guidance in making this thesis better.

I acknowledge Mr. Jim Sajewski at Mechanical Engineering, Mr. John Macek at Engineering Technology for being always ready to help out with any technical needs. Finally, I would like to thank my colleagues Ms. Hoda Parvin, Mr. Ravi Vayeda, Mr. Mahesh Sonawane and Mr. Yu-Hsuan Huang for their support all the time.

TABLE OF CONTENTS

Page

LIST OF FIGURES

FIGURE Page

FIGURE Page

FIGURE Page

LIST OF TABLES

CHAPTER I

INTRODUCTION

I.1 Hardness

The hardness of a metal is one of the most important mechanical properties. It can be classified into three major categories; namely scratch, static indentation, and dynamic or rebound. Indentation hardness characterizes the resistance of a material to permanent deformation or cutting. Indentation hardness testing mainly is used in engineering and metallurgy. Indentation hardness tests are carried out in almost all the manufacturing industries. The distinct advantages of such testing over other material characterization tests are as follows:

- Easy to perform.
- Quick (takes less than 30 sec) and little sample preparation required.
- Almost non-destructive and the finished parts can be tested without damage.
- A specimen of nearly any size or shape can be tested.

This thesis follows the style and format of ASME *Journal of Manufacturing Science and Engineering.*

Indentation hardness testing has been in practice for a long time. The first widely used and standardized testing method was developed in 1900 by the Swedish engineer J. A. Brinell; thereafter various hardness tests were established. Fig. 1.1 show two commercially available hardness testers that are known as Brinell and Rockwell testers respectively.

Fig 1.1: Brinell hardness tester (left) and Rockwell hardness tester (right)

The basic principle in most of the hardness tests is to characterize the hardness based on the shape of the impression made by an applied indentation load. The main difference

between the tests is the use of different indenter shapes, and indentation loads. Standard tables and charts for conversion between the scales are available. Table 1.1 lists a few of the indentation hardness tests, and the respective indenters.

Table 1.1: Commonly used hardness tests, and the indenters

Test	Type of indenter
Brinell hardness test	Spherical indenter
Meyer hardness test	Spherical indenter
Rockwell hardness test	Spherical and Diamond pyramid
Knoop hardness test	Diamond pyramid
Vickers hardness test	Square base diamond pyramid

I.2 Spherical indentation testing

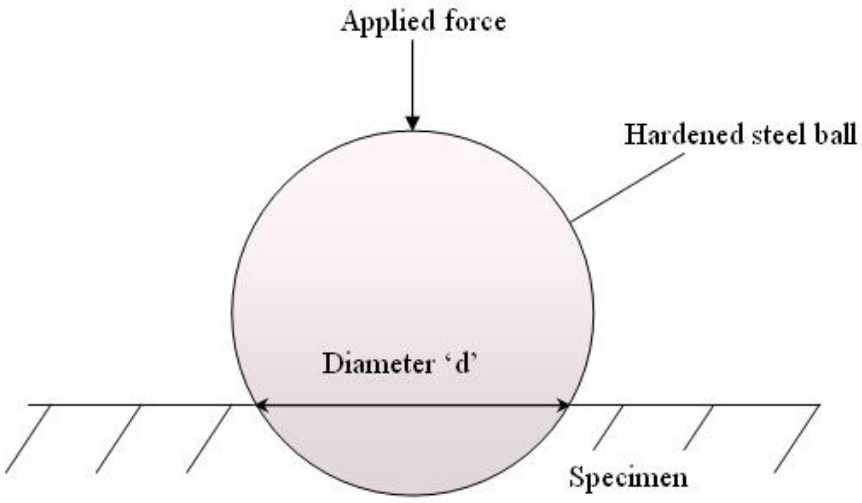

Fig. 1.2: A spherical indentation test

In the spherical indentation testing method, a spherical indenter or ball is pressed with a certain load against the material being tested, as shown in Fig 1.2. The *geometry* of a residual indentation is collectively defined by its diameter and depth. This information along with the applied load is used to predict the various properties of a material.

Table 1.2: Details of various hardness testers, and their testing parameters used for spherical indentation testing

Tester	**Scale**	**Indenter diameter**	**Indentation load (kgf)**
Rockwell	HRF	1.6 mm (1/16”)	60
Rockwell	HRB	1.6 mm (1/16”)	100
Rockwell	HRG	1.6 mm (1/16”)	150
Rockwell	HRH	3.2 mm (1/8”)	60
Rockwell	HRE	3.2 mm (1/8”)	100
Rockwell	HRK	3.2 mm (1/8”)	150
Rockwell	HRL	6.3 mm (1/4”)	60
Rockwell	HRM	6.3 mm (1/4”)	100
Rockwell	HRV	12.7 mm (1/2”)	150
Brinell	HB	1, 2.5, 5, 10 mm	500
Brinell	HB	1, 2.5, 5, 10 mm	1000
Brinell	HB	1, 2.5, 5, 10 mm	1500
Brinell	HB	1, 2.5, 5, 10 mm	3000

The standard practice is to use a hardened steel ball as the indenter in order to minimize the deformation of the indenter itself. The Brinell hardness testing method makes use of

a 10.000 (± 0.005) mm diameter hardened steel ball with a hardness value of 850 HV (Vickers hardness) or higher, and the Rockwell hardness testing method uses different indenters such as 1/16" (1.5875 mm) diameter or 1/8" (3.175 mm) diameter hardened steel balls according to the scale used in the test.

Table 1.2 provides the details of the various hardness testers, and their testing parameters that are used for spherical indentation testing. To test the hardness of a specimen, it is placed on the steel anvil of the testing machine. The surface of the anvil is polished in order to reduce the friction between the surfaces of the anvil and the specimen. The hardness of a material is determined using the spherical area of the indentation in the Brinell hardness testing method, and the projected area of the indentation in the Meyer hardness testing method. Both the *regular* and *superficial* Rockwell hardness tests use two different indentation loads, namely *major* and *minor*. The difference in the depths of the indentations produced by the loads is used to calculate the final hardness number.

There are different applications of the spherical indentation testing methods. These are used in the Brinell and Rockwell tests to find the hardness number of a material. A rough estimate of the ultimate tensile strength of a material can be made using the Brinell hardness number. Table 1.3 shows such estimates for aluminum alloys of different series.

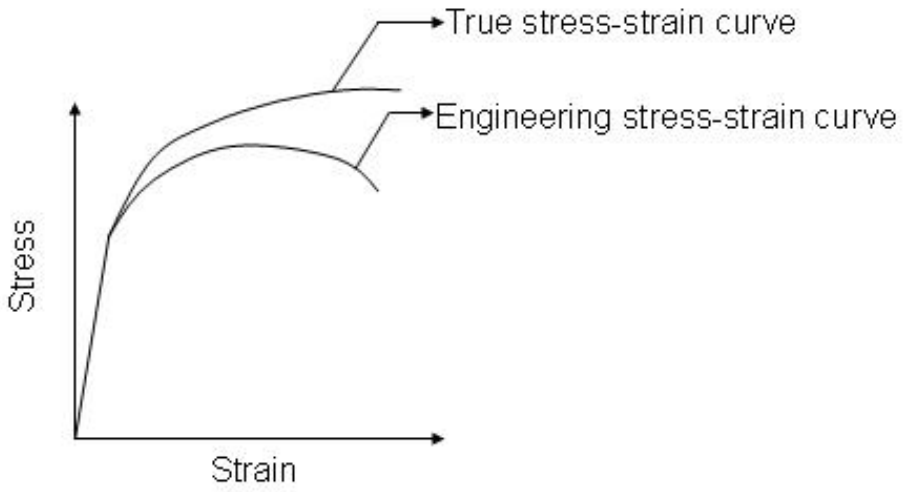

Fig. 1.3: Tensile test result showing engineering and true stress strain curves

The uniaxial tensile stress-strain curve as shown in Fig. 1.3 can be extracted using the data from the spherical indentation testing based on *Tabor's relations*. These relations determine the stress as a function of the average pressure below the indenter, and the strain as a function of the ratio of the diameter of the indentation to that of the indenter.

Since the standardized spherical indentation tests can be conducted easily and quickly, such tests usually are used to measure the effectiveness of various processes such as annealing, tempering, hardenability, heat treatments, surface treatment, and cold working on a material.

Table 1.3 Hardness relations for wrought aluminum alloys [1]

Ultimate Strength – Hardness Relationship for Wrought Aluminum Alloys

Principal alloying elements	Designation	Hardness range	Ultimate tensile strength
Copper	2000 series	(45 - 130) HB	σ = 580 HB
Copper	2000 series	(45 - 130) HB	σ = 555 HB + 2150
Manganese	3000 series	(28 - 77) HB	σ = 555 HB
Manganese	3000 series	(28 - 77) HB	σ = 522 HB + 1595
Magnesium	5000 series, temper 0	(28 - 65) HB	σ = 605 HB
Magnesium	5000 series, temper 0	(28 - 65) HB	σ = 617 HB – 557
Magnesium	5000 series, temper H	(36 - 105) HB	σ = 565 HB
Magnesium	5000 series, temper H	(36 - 105) HB	σ = 604 HB – 2580
Magnesium and Silicon	6000 series, tempers: 0, T1, T4	(25 - 90) HB	σ = 540 HB
Magnesium and Silicon	6000 series, tempers: 0, T1, T4	(25 - 90) HB	σ = 603 HB – 3210
Magnesium and Silicon	6000 series, tempers: T5, T6, T83, T831, T832	(60 - 120) HB	σ = 460 HB
Magnesium and Silicon	6000 series, tempers: T5, T6, T83, T831, T832	(60 - 120) HB	σ = 496 HB – 2910
Zinc	7000 series	(60 - 150) HB	σ = 554 HB
Zinc	7000 series	(60 - 150) HB	σ = 558 HB – 409

Ultimate Strength – Hardness Relationship for Cast Aluminum Alloys

Principal alloying elements	Designation	Hardness range	Ultimate tensile strength
Copper	204.0	(105 - 125) HB	σ = 200 HB + 36000
Copper	242.0	(70 - 110) HB	σ = 446 HB – 4465
Silicon and Copper	355.0	(65 - 105) HB	σ = 448 HB – 645
Silicon and Copper	356.0	(60 - 80) HB	σ = 556 HB – 6780
Silicon and Copper	390.0	(100 - 150) HB	σ = 511 HB – 24820
Zinc	771.0	(85 - 120) HB	σ = 292 HB + 13150

I.3 Spherical indentation testing on a sheet metal

A sheet metal has large surface area to thickness ratio. Generally, the thickness of a sheet metal is less than 5mm. Spherical indentation tests are used to test the hardness of sheet and strip metals that mainly are used for operations such as stamping. A spherical indentation test on a sheet metal rested on an anvil is shown in Fig. 1.4.

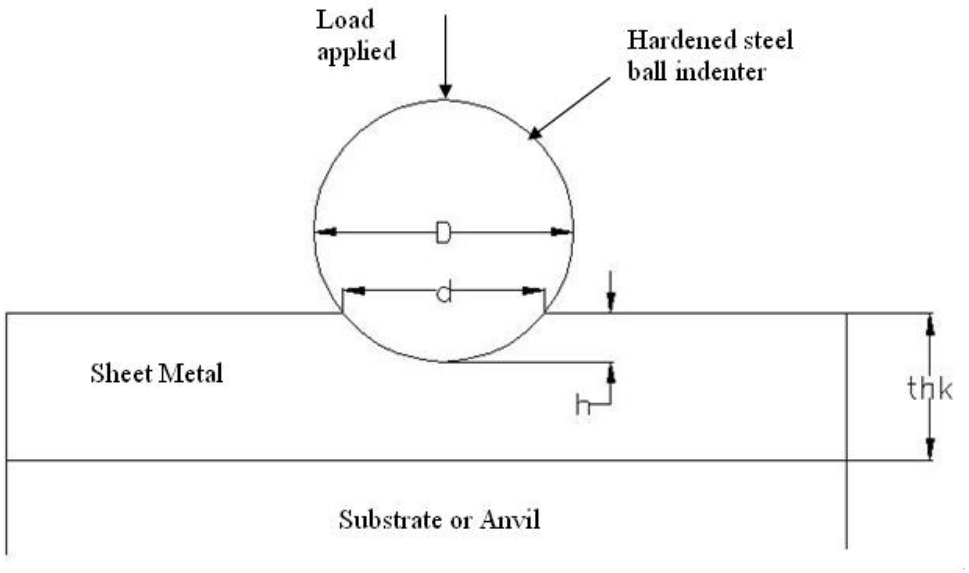

Fig. 1.4: A spherical indentation test on a sheet metal with an anvil support

The anvil normally is harder than the sheet metal to be tested. It is likely that the anvil will influence the test readings, as the thickness of the sheet metal may be insufficient to support the applied load. Such an influence is defined as the *anvil effect*, and is visible on the bottom side of a 2 mm thick aluminum sheet, shown in Fig. 1.5.

In order to avoid such flawed readings, a rule indicated by both ASTM standard E 10-27 [2] and British Standards Institute #240 (Part I) is followed. According to this rule, the thickness of the specimen should be more than ten times the depth of the indentation. ASTM also specifies that the limiting thickness should be such that no bulge or other marking appears on the side of the specimen opposite to the side of the impression [3]. In other words, if the depth of the indentation is more than one tenth of the thickness of

the sheet metal, then it is likely that the anvil has played a role in resisting the deformation. In these cases, the hardness number obtained from the spherical indentation test for the sheet metal does not represent the hardness of the metal alone. Rather, it represents the combined hardness values of the sheet metal and the anvil.

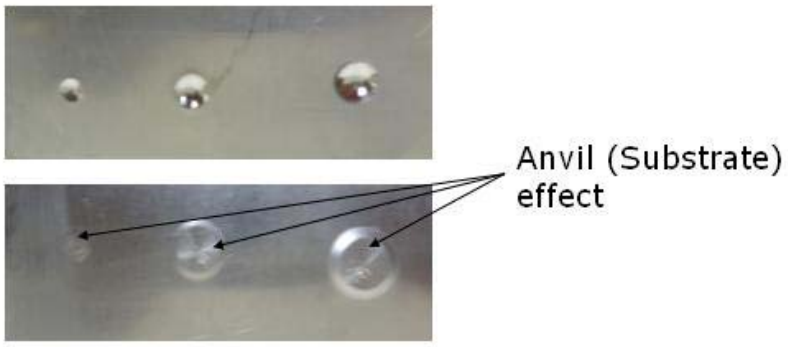

Fig. 1.5: Top and bottom sides of a 2 mm thick Al3003-H14 sheet metal with the indentation and the anvil effect

Generally, lower loads or smaller indenters are used to avoid the anvil effect on a sheet metal. Special hardness testing methods such as micro or nano indentation testing use such special loads and indenters. But the use of such methods is complicated, and results in a loss of the main advantage of standardized hardness testing methods, namely simplicity. In fact, such testing methods are extremely localized, require skilled labor, and are much more expensive than the conventional Brinell or Rockwell hardness testing methods. Moreover, these latter methods use large indenters which ensure that each impression covers many grains, and provides a better indication of the subsurface properties.

I.4 Research objective

The objective of this research is to investigate the anvil effect in spherical indentation testing on sheet metals. This effect arises due to excessive indentation load on the sheet metals, which produces significant depth of penetration in comparison with the original sheet metal thickness.

The effect of the sheet metal thickness on the geometry of the indentation for a constant load is evaluated. Ideally, if the load is unchanged, the geometry of the indentation should not vary with the thickness of the sheet metal; however, this is not what is observed in the presence of the anvil effect. Using experiments and finite element simulation, an investigation is carried out to study the anvil effect by varying identified parameters of the spherical indentation testing.

The experiments are conducted on sheet metals made of aluminum alloys which are used in the manufacturing industry Three such sheets having different thicknesses are used in this study. From the tensile test conducted on each of the sheets, it was found that they have very similar mechanical properties.

Further investigation is carried out by the numerical simulation of the spherical indentation test using the commercially available software ABAQUS. Tensile test results

of the aluminum sheets are supplied as the values of the properties of the material for the simulation. Experiments to find the coefficient of friction between the sheet metal and anvil are carried out. Displacement of a rigid indenter is given as an input to the simulation, and an indentation load is obtained in the form of a reaction. A numerical simulation gives better results if the boundary conditions are modeled as close to reality as possible. Stresses, strains, and reactions in the sheet metal and anvil can be analyzed with the help of such a simulation. It also becomes possible to find the finer details such as the different modes of deformation on metal sheets of different thicknesses during the indentation process.

The indentation response of a metal sheet is dependent on the level of the work hardening of that metal due to the process of rolling. Practically, it is difficult to produce metals with a desired strength and tensile test properties. In this research, the indentation response of such metals is investigated using the method of finite element analysis by varying their different material properties.

Throughout this research, the parameters used in the spherical indentation testing are analyzed in a dimensionless manner in order to generalize the end results. Normalized plots obtained at constant indentation pressures are fitted, and equations representing the effects of the anvil are formulated.

It is difficult to avoid the anvil effect on sheet metals when testing them on conventional hardness testing machines such as Brinell and Rockwell hardness testers with their available standard loads. Presently, the tests in which the anvil effect is found are considered invalid. Even the *one tenth rule* does not always help in avoiding this problem.

This problem is precisely the central focus of this research. We propose a method to rectify the readings obtained with the anvil effect using three parameters: the thickness of the sheet metal, the indentation load, and the indenter geometry. A simple procedure, based on an equation quantifying the anvil effect, is proposed to obtain the equivalent indentation depth of a bulk material for cases where such an effect is present. The upper and lower limits of the various testing parameters used in this procedure are also proposed, and within them, the results obtained are reasonably accurate.

CHAPTER II

LITERATURE REVIEW

II.1 Indentation hardness tests

The Brinell hardness testing methodology was introduced in 1900 [4]. For this testing, Brinell used a 10 mm diameter hardened steel ball to make the indentations on a specimen for 30 sec. For soft metals, he applied a load of 500 kgf, whereas for harder metals, he increased the load to 3000 kgf. The Brinell Hardness Number *(HB)* is calculated by dividing the load '*L*' by the surface area of the indentation as shown in the equation (2-1) where '*D*' is the ball diameter, and '*d*' is the indentation diameter.

$$HB = \frac{L}{\frac{\pi D}{2}\left(D - \sqrt{D^2 - d^2}\right)} \tag{2-1}$$

Meyer [5] proposed the idea of using the projected area of the indentation for calculating the hardness number *(HM)* instead of the surface area of the indentation. This makes calculation of a hardness number substantially simpler than the other methods as it can be seen from the equation (2-2).

$$HM = \frac{4L}{\pi d^2} \tag{2-2}$$

Unlike the other methods used for hardness testing, a third method known as the Rockwell [4] hardness testing uses two indentation loads. There are two types of Rockwell hardness tests, *regular* and *superficial*, which primarily differ in the loads applied, and the geometry of the indenters used. For the regular Rockwell hardness testing method, a minor load of 10 kgf is applied to set up a base or zero point. After this initial tuning, a major load of 60, 100 or 150 kgf is first applied, and then removed. In this method, the hardness number is inversely proportional to the depth of the indentation, and the indenters are shaped as diamond cones or hardened steel balls of various sizes.

II.2 Geometrically similar spherical indentations

ASTM Specification E10 [2] recommends the standard loads for the Brinell hardness testing method as listed in Table 2.1. It is noted that for a sample tested with three different loads, the Brinell hardness values are different [4]; hence, it is recommended to use geometrically similar indentations for a given material.

Table 2.1: ASTM Specification E10 for Brinell hardness testing [2]

Indenter diameter (mm)	**Indentation load (kgf)**	**Recommended Range**
10	3000	96 to 900 HB
10	1500	48 to 300 HB
10	500	16 to 100 HB

The load should be varied in a certain proportion to the diameter of the indenter in order to obtain geometrically similar indentations. The hardness number for a given material remains the same for geometrically similar indentations. As long as the contact angle '*A*' shown in Fig. 2.1 remains the same, the tests produce geometrically similar indentations. The condition for this is illustrated in the equation (2-3).

[Henceforth, in this thesis, the ratio L/D^2 is called as the *indentation pressure (P)*.]

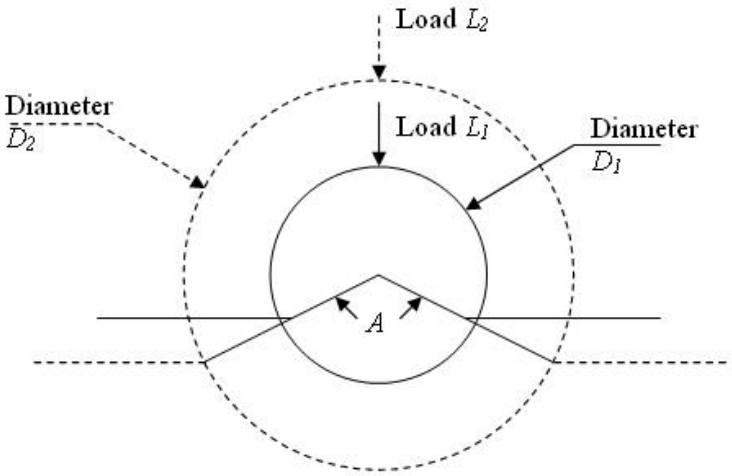

Fig. 2.1: Geometrically similar spherical indentations

$$\frac{L_1}{D_1^2} = \frac{L_2}{D_2^2} = \text{Constant} \qquad (2\text{-}3)$$

A load of 3000 kgf, and a spherical indenter of 10 mm diameter produce an indentation pressure of 30 kg/mm^2. The same value of indentation pressure can be obtained by using a load of 750 kgf, and a spherical indenter of 5 mm diameter [4].

II.3 Relation with the tensile test properties

The spherical indentation technique also can be used to determine the uniaxial tensile test properties of a material. There are different ways in which the stress-strain curve can be determined from the spherical indentation testing.

Three types of relations amongst various indentation parameters are commonly used to correlate to the properties of the tensile test [6]. These relations are: (1) mean pressure and contact radius, (2) force and contact radius, and (3) force and penetration depth.

The various properties of the tensile test can be estimated by observing the geometry of the indentation after unloading the material. In the seminal work by Meyer [5], he proposed that the relation between the load and the indentation diameter follow a power law as indicated in the equation (2-4).

$$F = Md^m \tag{2-4}$$

where M and m are material constants. Tabor [5] showed a direct relation between the indentation radius, diameter of the spherical indenter, and the plastic strain. He also specified the relation between the stress and the average pressure.

II.4 Indentation on sheet metals and thin films

In order to conduct indentation hardness tests on sheet metals, the minimum sample thickness guidelines as given in ASTM E10 and E18 [2] should be followed. The minimum sample thickness depends on the load and the hardness of the material. The rule of thumb recommends that the depth of indentation should be less than 1/10 of the thickness of the sample sheet metal. In other words, this rule suggests that the sample thickness should be greater than 10 times the depth of the indentation. This does not always ensure the absence of the anvil effect.

In one of the earliest works related to this area, Kenyon R. L. studied the effect of the thickness on the accuracy of the Rockwell hardness testing method on thin sheets [7]. He also worked on the effect of the surface preparation by conducting the tests on both etched and polished materials. For the polished samples, he found that even when the thickness of the sheet metal decreases, the hardness readings remain constant. But after a certain threshold thickness is reached, a bulge appears on the other side of the sample, i.e., the anvil effect becomes apparent; thereafter, the hardness readings are lower than

the previous cases. Kenyon's study was aimed at finding the minimum thickness of the material for which the anvil effect does not arise.

Heyer R. H. [8] investigated *pile up* and *sinking in* around the indentation, and showed their connection with the minimum thickness of the sheet metal used in the Brinell hardness testing method. Waters N. E. [9] studied the indentation of vulcanized rubber sheets of different thicknesses using a rigid spherical indenter. He found that the results of this study fit a modified form of the *Hertz contact solution* for the indentation of a ball into a semi-infinite elastic medium. Lebouvier D. et al. [10] derived the kinematic solution for the plane strain wedge indentation of a rigid perfectly plastic semi-infinite bi-layer system, and found that the critical ratio of the layer thickness to the wedge indentation width is influenced by the anvil.

Taylor D. J. et al. [11] performed experiments on thin soft coatings of gelatin gel on a rigid supports to determine the effect of layer thickness on an elastic response when indented with a relatively large spherical indenters. They found an expression giving the relation between the rigidity modulus, the indentation load, the layer thickness, and the radius of the spherical indenter. In his study of the indentation of elastic layers, Pitts E. established the relations between the depth of indentation, the indenter shape, the elastic constants of the layer, and the load applied for thick and thin elastic layers indented by an axi-symmetric rigid spherical indenter [12]. He compared the available experimental results, and provided the conditions necessary for the application of his theory.

Thus, most of the previous investigations are directed towards finding the limiting thickness of sheet metals or thin films in order to avoid the error introduced by the hardness of the anvil. The rule of thumb, also known as the 'one tenth rule', for determining the thickness of the sheet metal is not always reliable. Experiments by Kenyon [7] showed that the ratio of the limiting thickness to the depth of indentation varies significantly. In some cases, it is as low as 6, whereas in others, it is more than 10. Although detailed charts and tables that list the values of the critical thickness for different test and metals are commonly available, as per the author's knowledge, no study has been carried out to date to rectify the error introduced due to the anvil effect in calculating the hardness number of a sheet metal in the spherical indentation test. Consequently, there is no procedure available to obtain the equivalent properties of a bulk material for the test performed on its sheet metal when the anvil effect arises. This research attempts to understand and quantify the anvil effect, and can be used to correct the readings affected by the anvil effect, and in turn, enable the use of macro hardness testers.

Recently, a lot of research has been conducted on hard anvils coated with thin films. In [13], Yang derived the closed form solutions for the load-displacement relationship and the contact stiffness as a function of the ratio of the contact stiffness to the film thickness and the material properties for an incompressible elastic thin film indented by a rigid spherical and conical indenter. He found that for frictionless boundary conditions between the film and anvil, the contact stiffness is proportional to the film thickness.

Yoo et al. [14] used the finite element method to investigate the effect of the radius of a spherical indenter on the critical indentation depth of a hard thin film to avoid the influence of a soft anvil. They observed that critical indentation depth decreases as the ratio of the indenter radius to the film thickness increases. In their numerical simulation, they used a rigid spherical indenter instead of a deformable indenter since there is no appreciable difference that it makes on the geometry of the indentation. The contact between the indenter and the film was assumed to be frictionless. Panich N. et al. [15] also used the method of finite element analysis to investigate the comparison of the penetration depth with the indentation response caused by a conical indenter acting on a hard anvil coated with soft material. Chaiwut Gamonpilas et al. [16] studied the effects of the changing anvil properties on the conical indentation in coated systems. They used a parametric study to find the ratio of the critical indentation depth to the coating thickness below which the anvil material has negligible influence on the indentation response.

All the investigations related to thin films deposited on an anvil differ from the indentation test on metal sheets in the length scale. I. Sridhar et al. [17] observed that at a very small scale, such as a nano-scale, the forces of adhesion between the indenter and the thin film play an important role in the deformation process. Since at such small scales the films are deposited on the anvil, the indentation response is significantly different from that found in the hardness testing of the sheet metals. Thin films bonded to the anvil do not lose contact with the anvil due to the indentation.

CHAPTER III

EXPERIMENTAL STUDY

Depending on the load applied and indentation geometry obtained, spherical indentation testing methods can be classified into three broad categories: macro, micro, and nano scaled. Macro-hardness testing is the simplest and quickest method used to obtain the mechanical properties of the material. This type of testing is widely used in the quality control of surface treatment processes.

The experimental study was conducted using the spherical indentation testing method identifies the anvil effect. Experiments were conducted on sheet metals made of two general purpose aluminum alloys: *Al3003-H14* and *Al6061-T6*. The major alloying elements in Al3003-H14 are: 1.2% of manganese and 0.12% of copper (all by weight). The major alloying elements in Al 6061-T6 are: 1% magnesium, 0.6% silicon, 0.28% manganese, and 0.2% chromium (all by weight). The details for the heat treatment process or *tempering* are indicated by the extensions T6 and H14.

The alloy Al3003-H14 has excellent corrosion resistance and good formability, and is commonly used in sheet metal working and in the manufacturing of chemical and food processing equipments, tanks, and heat exchangers. Similarly, the alloy Al6061-T6 has a fine combination of high strength, high corrosion resistance, and good machinability.

III.1 Spherical indentation tests on the sheet metals

The indentation tests were carried out on three different sheets made of Al3003-H14 and Al6061-T6 sheets. The thickness of the three sheets was 0.813mm (0.032”), 1.27mm (0.05”), and 2.03mm (0.08”) respectively.

III.1.1 Procedure of spherical indentation testing

The Brinell hardness testing machine and the automatic Rockwell hardness testing machine shown in Fig. 1.1 were used to carry out the indentation tests. Multiple indentations were made on the same sheet metal using different indentation loads applied for 30 sec at different locations. The loads were increased stepwise as per the following list: 15, 30, 45, 60, 100, 150, 500, 1000, and 1500 kgf. To make the indentations, two hardened steel ball indenters were used. Their diameters are 3.175mm and 10mm respectively. The diameter and depth of the indentation was measured using an OLYMPUS optical microscope shown in Fig. 3.1. This instrument is a measuring microscope, and has a very fine resolution of 0.0001mm in the X, Y, and Z directions. The depth of the indentation was measured by focusing it on the bottom and top of the spherical indentation. The anvil used in all the experiments was flat and cylindrical, and was made of steel.

Fig. 3.1 Optical microscope used for measuring the geometry of indentation

III.1.2 Experiment results

As the load of the indentation was increased, a mark started to appear on the sheet metal on the side of the anvil. For example, on the sheet metal specimen made of Al3003-H14, and having the thickness of 0.8128mm, the mark started to appear at the load of 30 kgf, and became more apparent with the increase in load as it can be seen in Fig. 3.2.

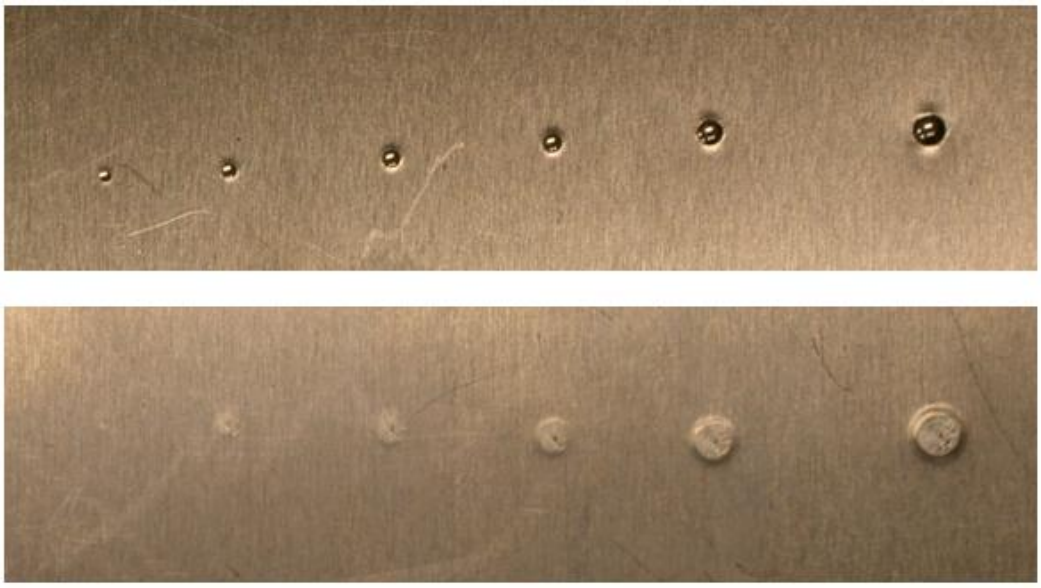

Fig. 3.2: Top and bottom sides of the 0.813mm thickness Al3003-H14 sheet indented from left to right with loads of 15, 30, 45, 60, 100, and 150 kgf respectively using a 1/8" diameter indenter

The surface texture of the as received aluminum sheets indicated their direction of rolling. [In this thesis, the *longitudinal direction* of rolling is considered to be the direction along the observed thin texture lines on the surface of the as received sheet metal, and the *transverse direction* of rolling is considered as the direction perpendicular to it.]

As it can be seen from Fig. 3.3, the shape of the indentation observed under the microscope is not perfectly circular but is rather elliptical. The maximum difference in the major and the minor diameter of the ellipse observed amongst the indentations in all the experiments was 0.02 mm. The shape of indentation was elliptical for all the loads,

and both the materials with its diameter being larger in the longitudinal direction than in the transverse direction. From this fact, it can be inferred that the elliptical shape of the indentation is caused by different amounts of springback in the two directions which arises after the removal of the indentation load; hence, the material properties (and, as discussed later, the tensile properties) must be different in the longitudinal and transverse directions. Henceforth, only the properties in the longitudinal direction are considered in this thesis. The depth of indentation is measured as the vertical distance between the center of the impression and the edge of the crater.

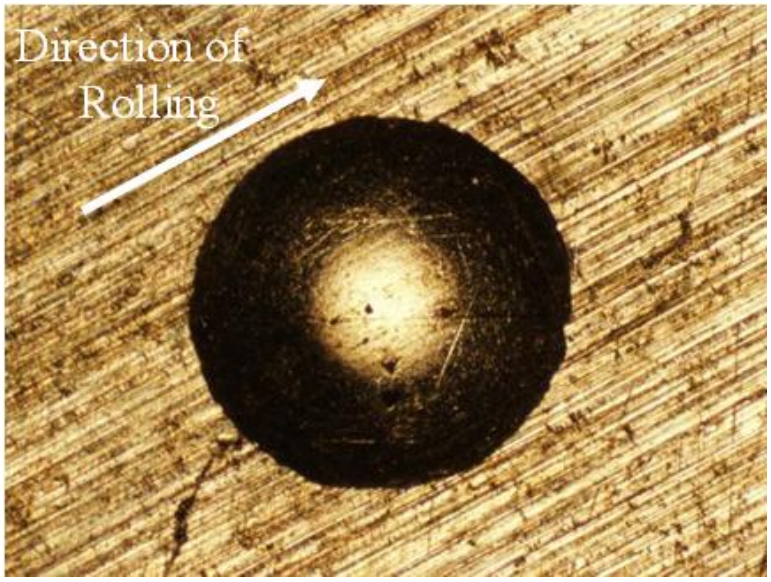

Fig. 3.3: Indentation on the 0.813 mm thick Al3003-H14 sheet metal showing the elliptical profile

The diameter and depth of the indentation measured on the three Al3003-H14 sheets vary along with the load as shown in Fig. 3.4 and Fig 3.5 respectively. If the same

indentation load is applied, then, the diameter of the indentation should remain unchanged regardless of the thickness of the sheet metal. But the observations made in the experiments were contrary to this intuition, and it was found that the diameter of indentation was different for different thickness sheets indented with the same load. Also, the difference in the diameters of the different indentations increased with the increase in the indentation load. For the sheet metal specimen having the smallest thickness, the diameter of the indentation was larger than that observed for the thickest specimen indented with the same load.

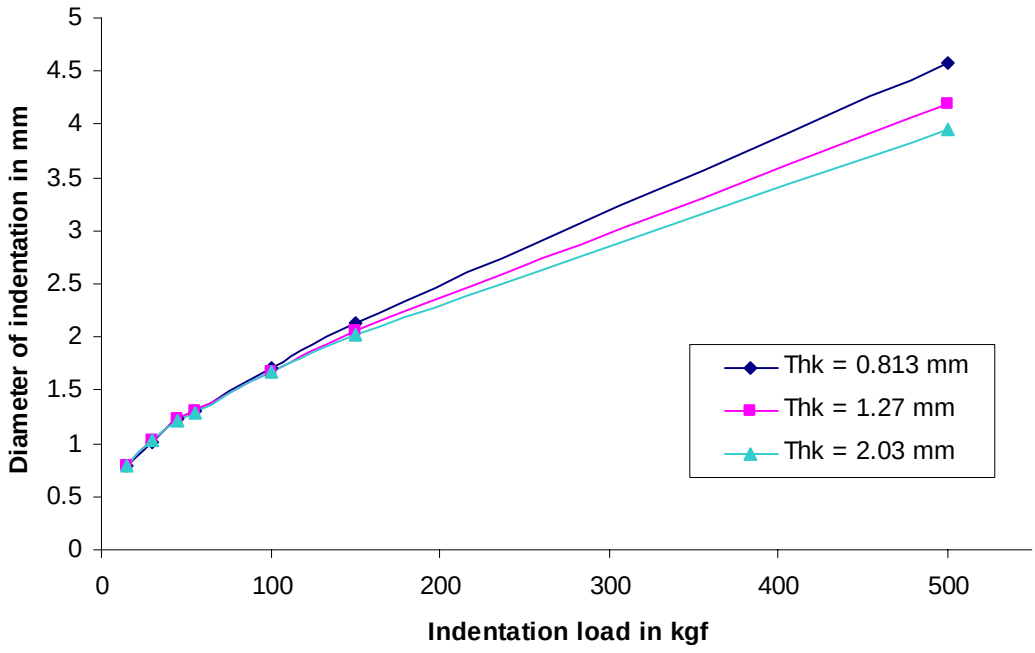

Fig. 3.4: Variation of the diameter of indentation with the load on three Al3003-H14 sheets

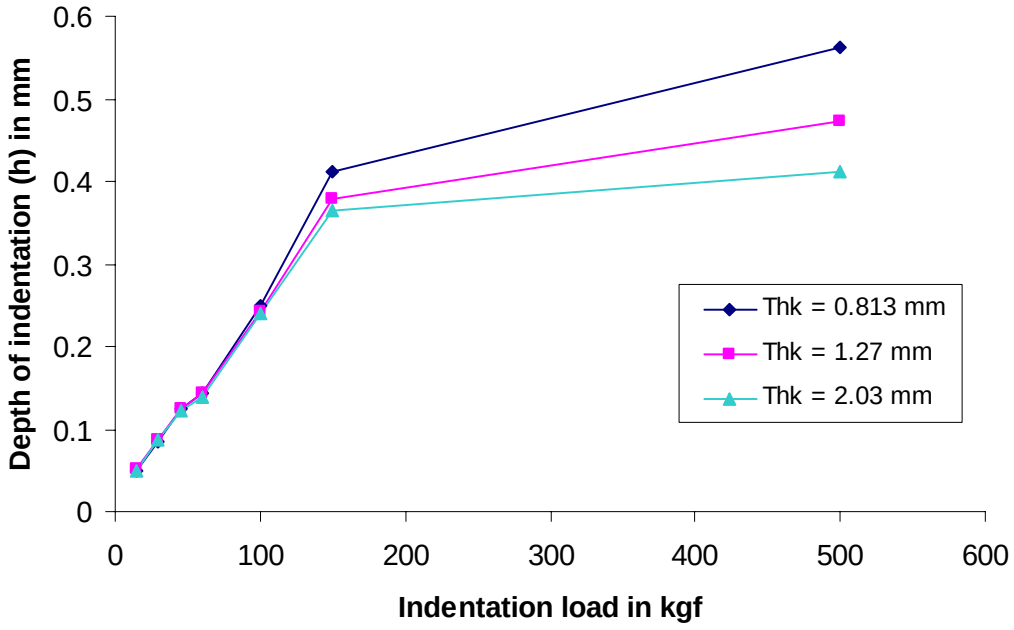

Fig. 3.5: Variation of the depth of indentation with the load on the three Al3003-H14 sheets

In Fig 3.5, the first six loads are applied using the 1/8" diameter indenter, and the last load is applied using the 10mm diameter indenter. A similar trend, as shown in Fig. 3.6, was seen in the Al6061-T6 sheets. The indentation diameter readings were smaller than the Al3003-H14 for the same load since the Al6061-T6 alloy is harder than the Al3003-H14 alloy. In Fig 3.7, the first six loads are applied using the 1/8" diameter indenter, and the remaining loads were applied using the 10mm diameter indenter.

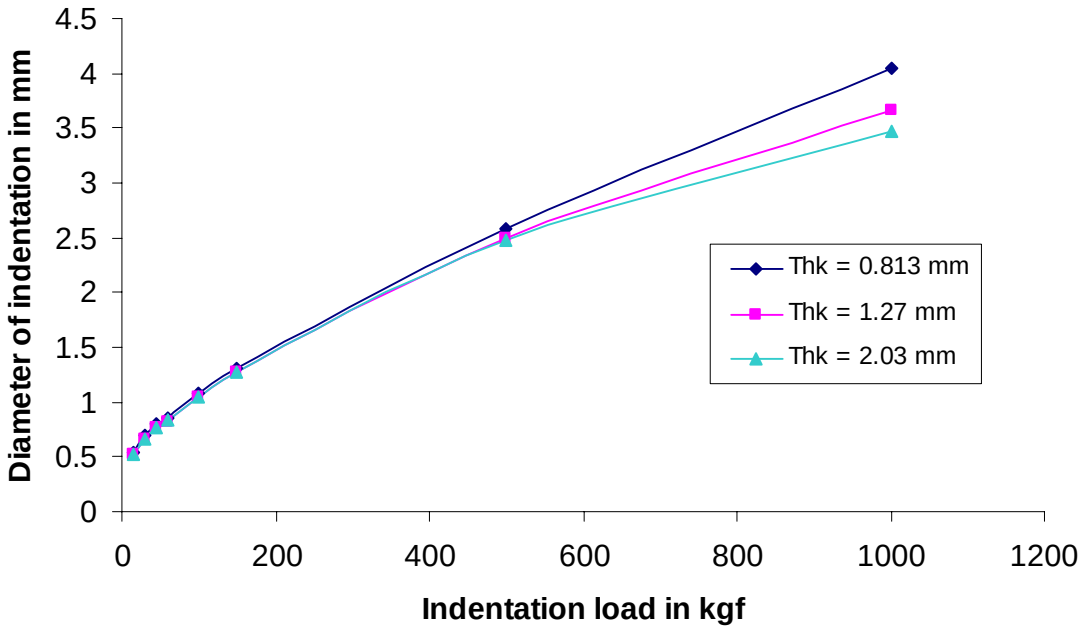

Fig. 3.6: Variation of the diameter of indentation with the load on three Al6061-T6 sheets

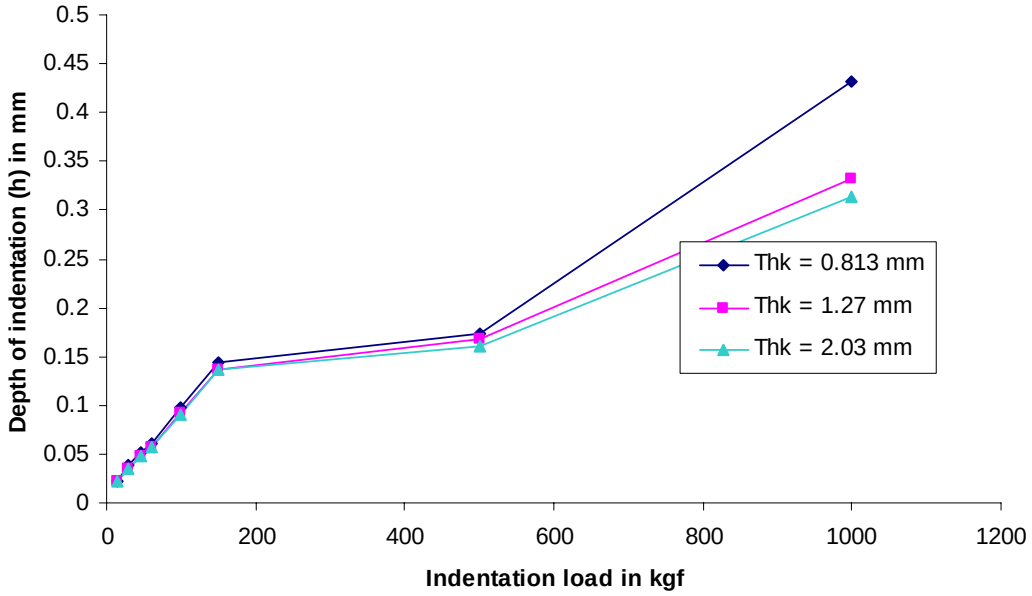

Fig. 3.7: Variation of the depth of indentation with the load on three Al6061-T6 sheets

III.1.3 Uncertainty analysis for the indentation experiments

The readings of the diameters and depths of the indentations show small variations, and can contain measurement errors. Uncertainty analysis can be used to model such variations and appropriately estimate the errors.

The overall uncertainty associated with the experiments is calculated as follows:

$$U_x = \left(B^2 + P_x^{\,2}\right)^{1/2} \tag{3-1}$$

where B is the *Bias limit* or *calibration error* and P_x is the *precision limit* or *random error*. In the analysis carried out in this research, the value of B is taken as the least count of the microscope which is 0.0001mm.

The precision limit is calculated as:

$$P_x = tS_x \tag{3-2}$$

where, the variable t is a function of the number of the sample readings N and the confidence level C. For $N = 5$ and $C = 90\%$, the value of t is 2.132.

Also, S_x is the sample standard deviation formulated as:

$$S_x = \sqrt{\frac{1}{N-1}\sum_{i=1}^{N}\left(X_i - \overline{X}\right)^2} \tag{3-3}$$

Table 3.1 shows the uncertainty error calculated for the diameter and depth of the indentation on the Al3003-H14 sheet metal having a thickness of 0.813mm.

Table 3.1: Indentation data with the uncertainty analysis on the 0.813mm thick Al3003-H14 sheet metal

Load (kgf)	Avg. Dia (mm)	Std. deviation (mm)	Uncertainty (mm)	Avg. Depth (mm)	Std. deviation (mm)	Uncertainty (mm)
15	**0.7877**	0.003552	0.007574	**0.0496**	0.004374	0.009326
30	**1.018**	0.003718	0.007928	**0.0843**	0.004049	0.008634
45	**1.2241**	0.003918	0.008355	**0.1237**	0.004115	0.008773
55	**1.3086**	0.004629	0.009870	**0.1426**	0.003842	0.008191
100	**1.7056**	0.004374	0.009326	**0.2505**	0.003384	0.007215
150	**2.1252**	0.004049	0.008634	**0.4106**	0.003371	0.007188
500	**4.5791**	0.004115	0.008773	**0.5619**	0.002678	0.005711

The maximum value of uncertainty obtained in all the readings was 0.01033 mm.

III.2 Tensile tests

From the indentation experiments, it can be observed that the effect of the anvil is related to the thickness of the sheet metal. Therefore, tensile tests were carried out on the

Al3003-H14 sheets of different thicknesses according to the well known standard ASTM B557M used for tensile testing of aluminum. For the purpose of testing, tensile test coupons were cut out of the sheets in longitudinal and transverse directions.

The true stress-strain curve of the material obtained from the tensile test is shown in Fig. 3.8. The tensile test results were used as values of the various material properties for the finite element simulation. Similar tests were also carried out on the Al6061-T6 sheets of different thicknesses. The alloy Al3003-H14 contains 1.2% manganese by weight. The addition of manganese increases the strength, and reduces the ductility of the alloy.

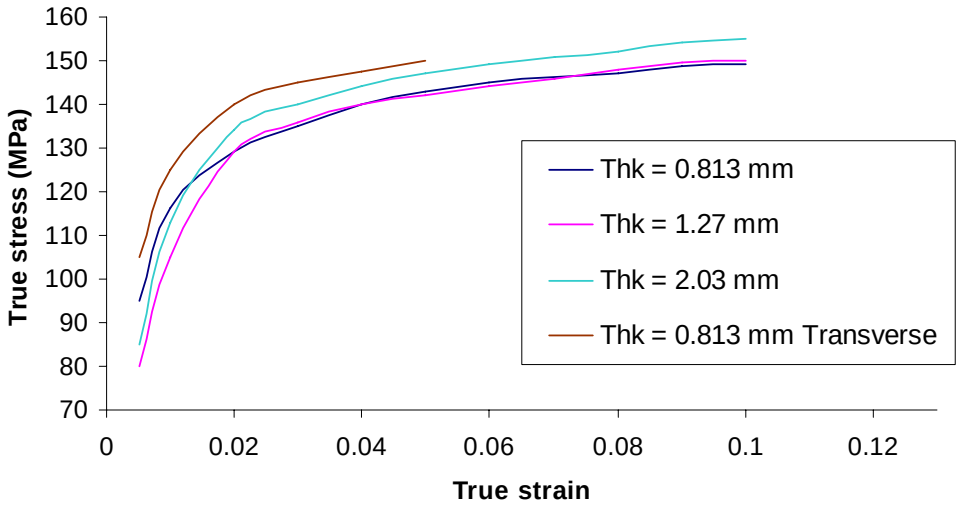

Fig. 3.8: Tensile test results of Al3003-H14 sheets

The properties of the sheet metals in the longitudinal direction show higher ductility and lower yield strength than those in the transverse direction. Since there was no significant

difference in the properties of all the sheets in the longitudinal direction, it was assumed that all the sheets came from the same batch and had similar material properties.

III.3 Metallographic tests

A metallographic study was carried out to see the microstructure of the cross section of the indented Al3003-H14 sheet metal. The specimen was polished to 0.05 μ and then etched using a reagent containing 100ml of distilled water, and 5ml of dilute hydrofluoric acid (40%). The oxide layer formed over the surface of the aluminum makes it difficult to see the grain boundaries; however, the particles of manganese are clearly visible in the matrix of aluminum. The distribution and alignment of these particles can be used to identify the different aspects of indentation such as the direction of the deformation of the metal due to indentation, and the density of material exactly below the indentation. Various locations in the cross section, taken along the longitudinal direction, were observed under the OLYMPUS optical microscope. These are shown in Fig. 3.9.

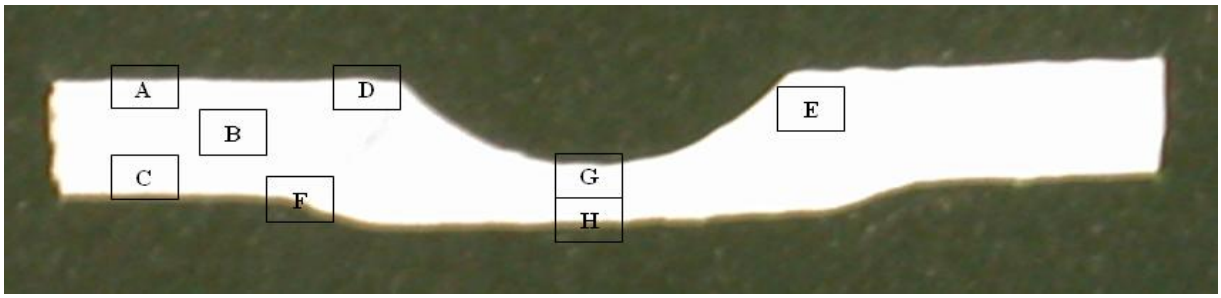

Fig. 3.9: Cross section of the indentation showing different locations

1) Locations A, B, and C

At the location A, the particles are densely packed near the surface, and become sparse near the subsurface locations as seen in Fig. 3.10, Fig. 3.11, Fig. 3.12, and Fig. 3.13. When the cross section of the sheet metal specimen is seen by the naked eye, a layer at the mid section of the thickness of the sheet can be seen. This layer has sparsely distributed and slightly elongated particles which can be seen using the microscope under magnification as seen in Fig. 3.12. The elongation of particles is due to the process of rolling which indicates that the material is compressed because of rolling, and has different properties at different layers of thickness as seen in Fig 13. Thus, if a micro or nano-indentation hardness test is carried out on this sheet metal, then it will not represent the true properties of the material as it will not be able to penetrate below the surface sufficiently.

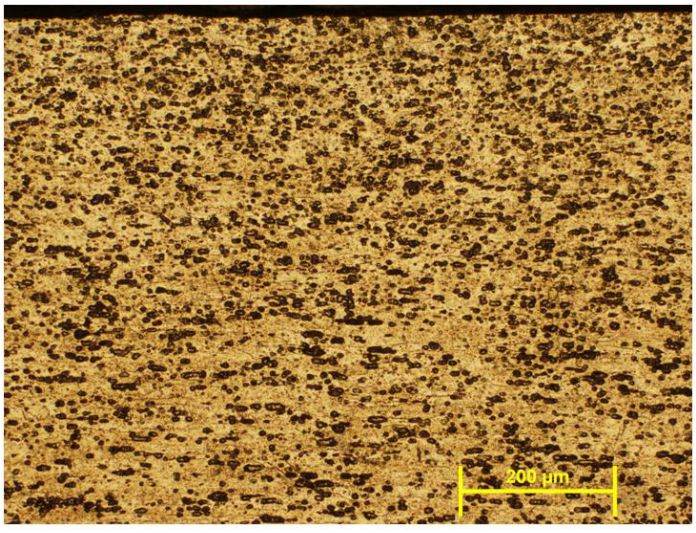

Fig. 3.10: Microstructure at the location A, 100 X

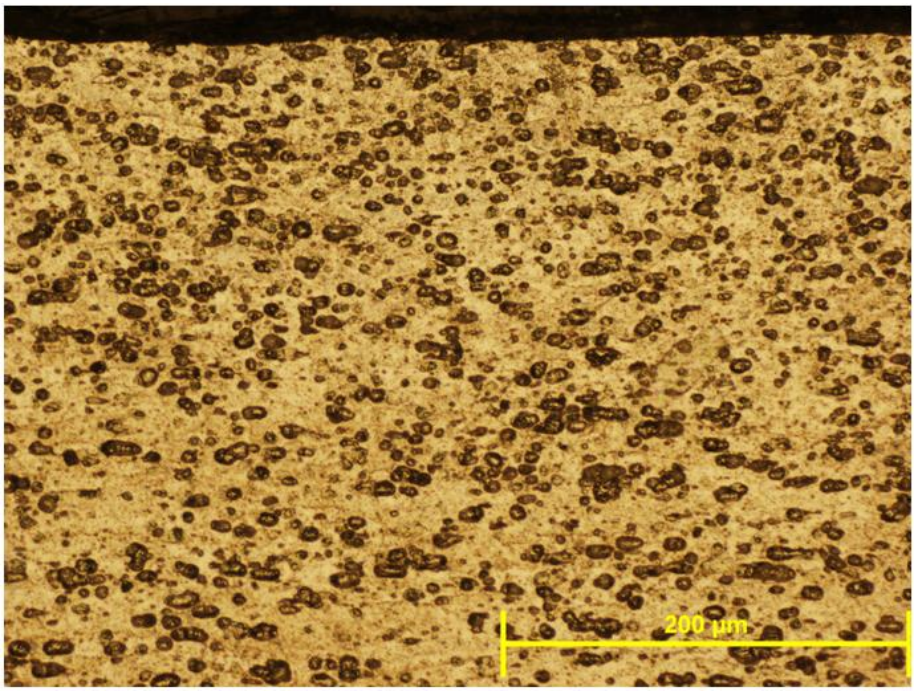

Fig. 3.11: Microstructure at the location A, 200 X

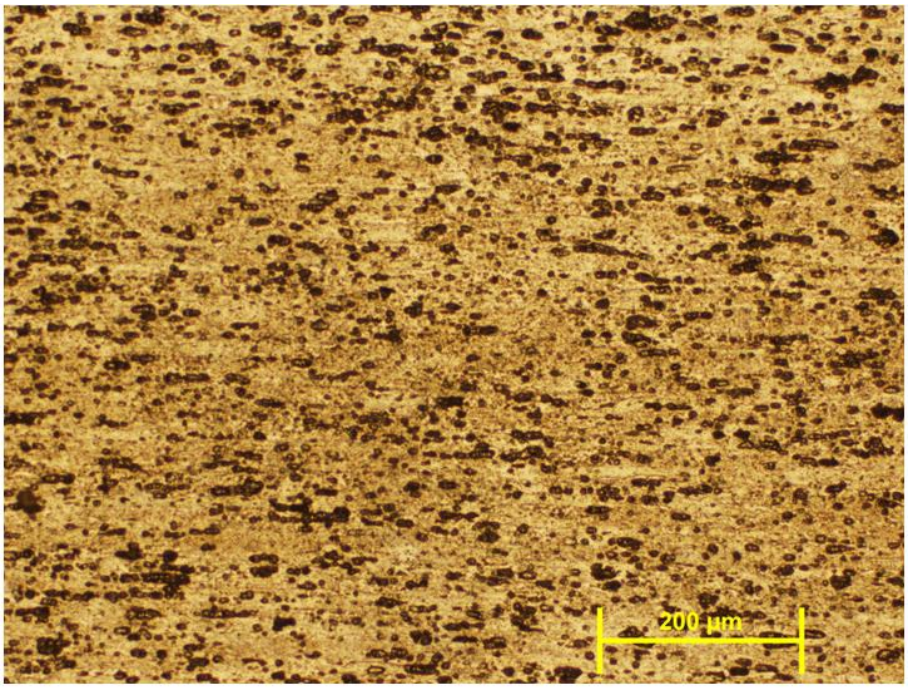

Fig. 3.12: Microstructure at the location B, 100 X

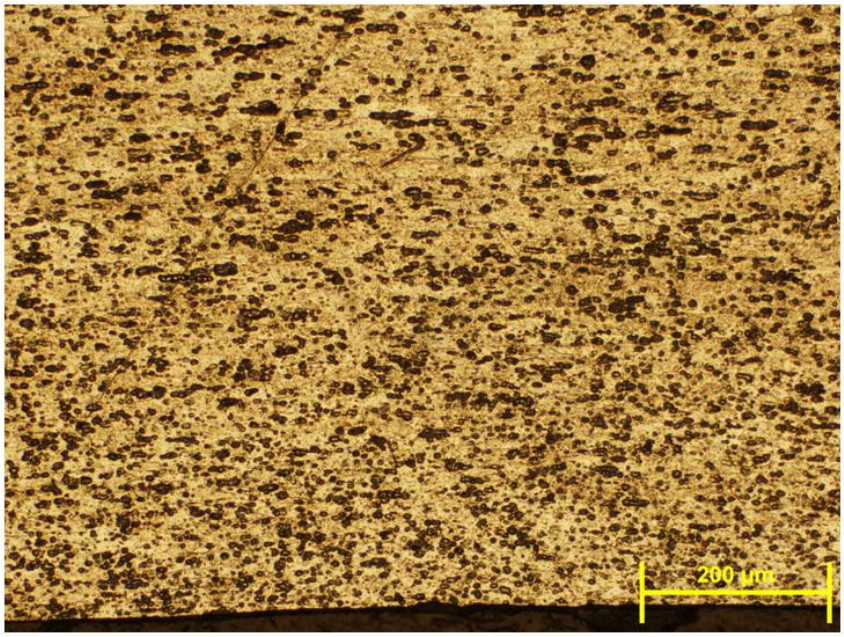

Fig. 3.13: Microstructure at the location C, 100 X

2) Locations D, E, and F

Looking at the particles, the flow of material due to the indentation is clearly visible in Fig. 3.14. The elongated particles are directed along the deformation due to the indentation as seen in Fig. 3.15, Fig. 3.16, and Fig. 3.17. The material below the indentation is large enough to cover many particles. This ensures the results reflect an average response of the bulk. The properties of the individual particles may be different than the average properties of the metal.

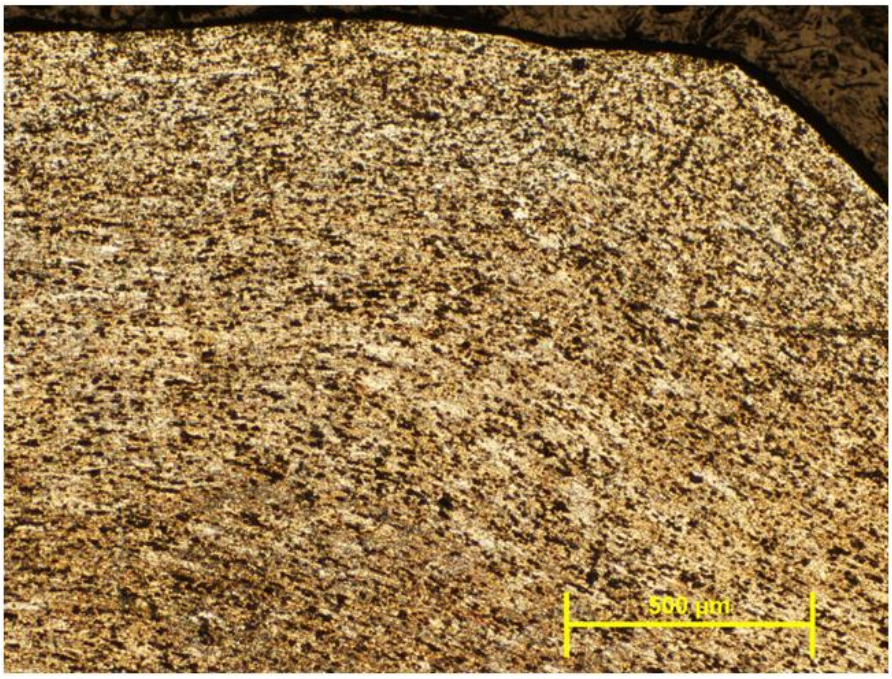

Fig. 3.14: Microstructure at the location D, 50 X

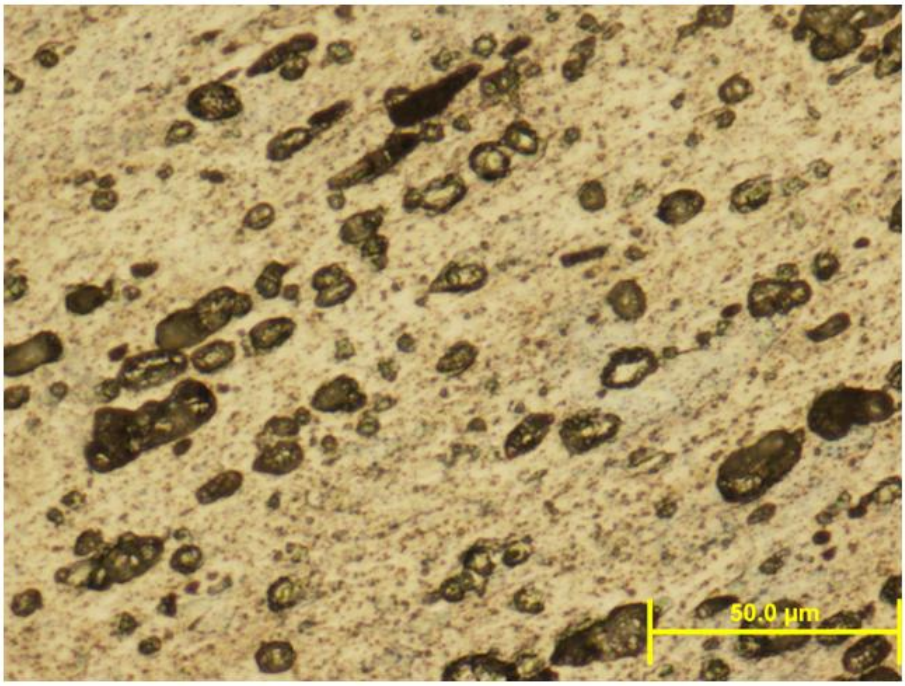

Fig. 3.15: Microstructure at the location E, 500 X

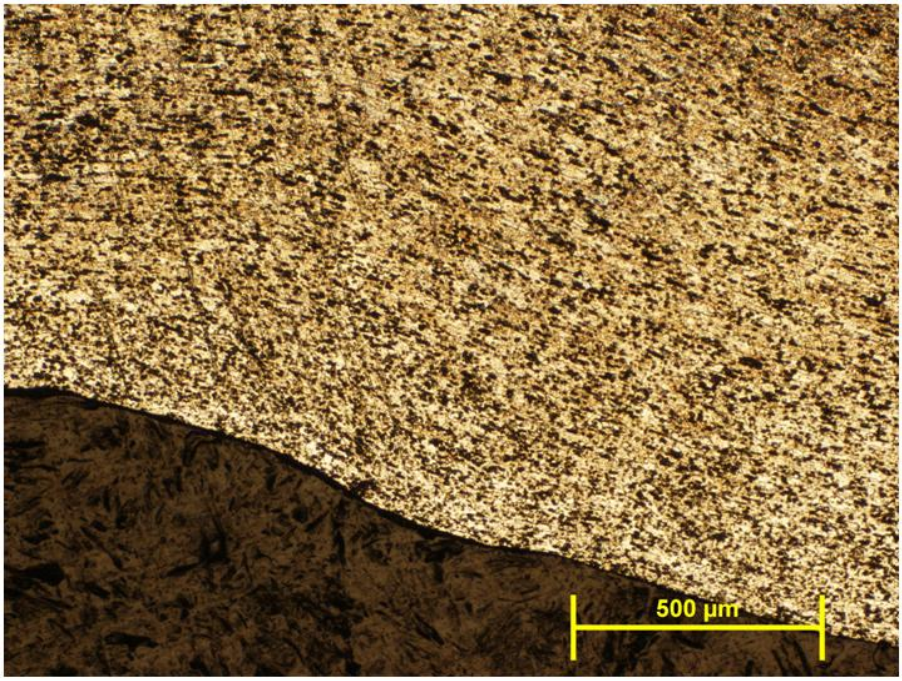

Fig. 3.16: Microstructure at the location F, 50 X

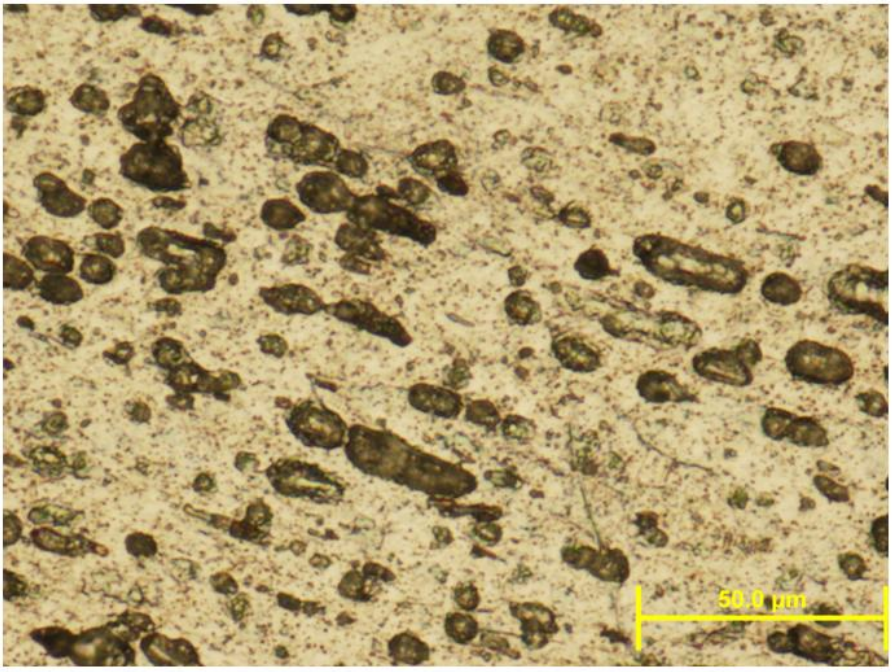

Fig. 3.17: Microstructure at the location F, 500 X

3) Locations G and H:

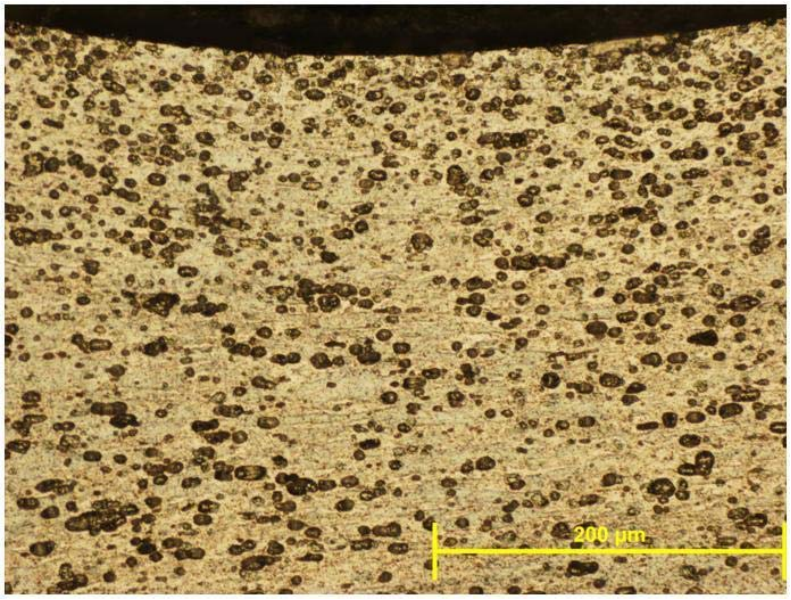

Fig. 3.18: Microstructure at the location G, 200 X

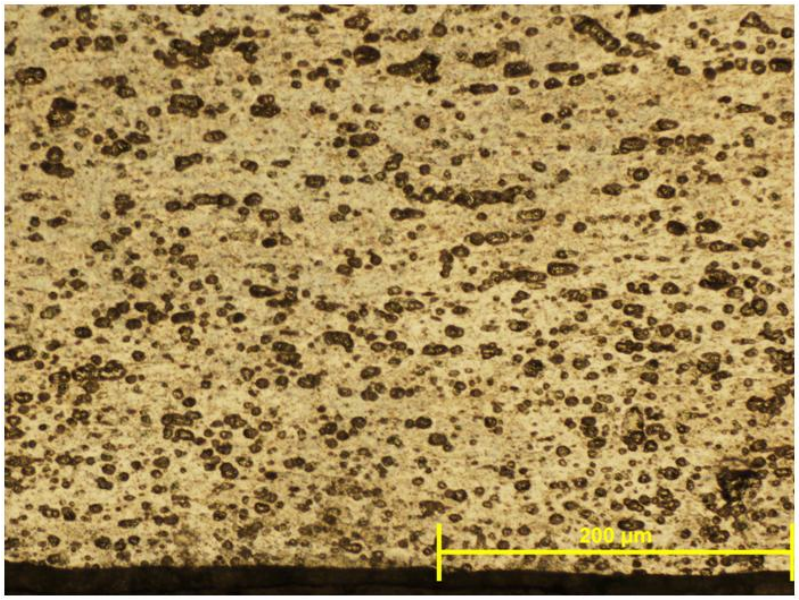

Fig. 3.19: Microstructure at the location H, 200 X

The region below the indentation shows a higher density of the particles near the surface; however, in the region below the indentation and near the center, the density of these particles reduces rapidly as can be seen in Fig. 3.18 and Fig. 3.19. This indicates that the flow of the material exactly below the indentation is radial and outwards.

III.4 Experiment to determine the coefficient of friction between the sheet metal and the anvil

The friction between the sheet metal and the anvil is an input to the finite element simulation; hence, it is essential to find out the coefficient of friction between them. The static coefficient of friction between the aluminum sheet metal and the steel anvil was measured using a simple experiment as shown in Fig 3.20. The anvil was tilted until the aluminum sheet began to move.

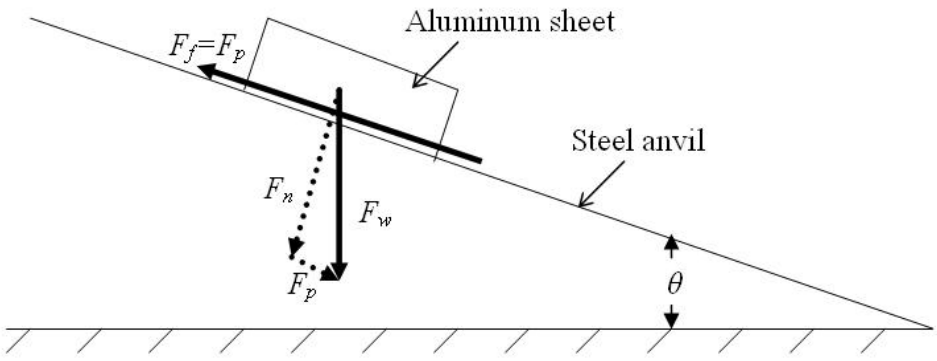

Fig. 3.20: A friction test showing the various forces and their components

The different variables present in the system are as follows:

F_w is the weight of the sheet metal,

F_p is the component of F_w parallel to the sheet metal,

F_n is the component of F_w perpendicular to the sheet metal ,

F_f is the frictional force.

θ is the angle of tilt of the anvil, measured in degrees.

The value of coefficient of friction (μ_s) is defined as:

$$\mu_s = \frac{F_f}{F_n} = \frac{F_p}{F_n} \tag{3-4}$$

Thus, substituting the values of F_p and F_n in the equation (3-4), the value of μ_s obtained is:

$$\mu_s = \frac{F_w(\sin\theta)}{\sqrt{F_w{}^2(1-\sin^2\theta)}} \tag{3-5}$$

And solving the equation (3-5), we obtain:

$$\mu_s = \tan\theta \tag{3-6}$$

In the experiments on the Al3003-H14 sheet, the value of θ was found to be close to 14˚ (± 0.5˚). The corresponding values of the coefficients of friction are given in Table 3.2.

Table 3.2: Values of the static coefficients of friction for

the Al3003-H14 sheet placed on the steel anvil

F_w (N)	Θ(˚)	μ_s
7.664	13.5	0.240
7.664	14	0.249
7.664	14.5	0.259

For the Al6061-T6 sheet, the value of θ was approximately 12˚ (± 0.5˚). The corresponding values of the coefficients of friction vary from 0.203 to 0.222.

CHAPTER IV

FINITE ELEMENT SIMULATION OF SPHERICAL INDENTATION

Finite element modeling was used to simulate the process of indentation numerically using the commercially available software ABAQUS. The aim of this study was to investigate the details of the process which cannot be determined experimentally.

IV.1 Finite element model

A two dimensional, axi-symmetric finite element model was developed for this analysis. Fig. 4.1 shows the boundary conditions and the mesh for the model. The process of indentation produces severe nonlinear geometries. For such geometries, higher aspect ratios need to be avoided [18]. Therefore, quadrilateral elements, in the form of squares, were used as the elements of the mesh.

The model shown in Fig. 4.1 has a 3.175 mm diameter indenter, and a 0.813 mm thick sheet metal placed on an anvil. The material properties for the sheet metal are for Al3003-H14 and that for the anvil are for steel. The indenter used in the spherical indentation testing is usually of high modulus and high strength. For the Brinell hardness testing method, the indenter is a hardened steel ball with a Vickers hardness of 850 or more. This indenter can be used on the material with a Brinell hardness of 450 or less.

The Al3003-H14 and Al6061-T6 sheets used in the experimentation had a Brinell hardness of 40 and 95 respectively, and this would have caused negligible deformation of the indenter in comparison with the deformation of the sheet in practice; therefore, in the simulations, a non-deformable or rigid indenter was used accordingly.

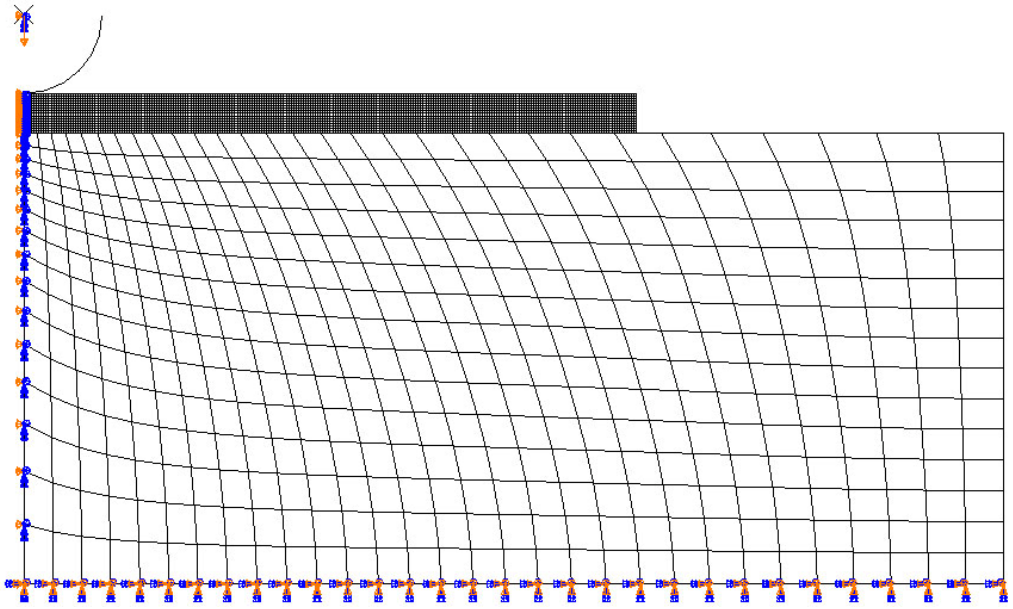

Fig. 4.1: Finite element model showing the boundary conditions and the mesh

In order to cover sufficiently the span of effect due to the indentation, the radius of the sheet metal was modeled as being more than 7.5 times the radius of the indenter. Similarly, the radius of the anvil was modeled as being more than 12 times that of the indenter, and the thickness of the anvil was modeled as being more than 12 times that of the sheet metal. The contact between the indenter and the sheet metal was assumed to be frictionless throughout the simulation. The contact between the sheet metal and the anvil

was initially assumed to be frictionless, and the effect of the friction on the indentation was studied later by varying the coefficient of friction between them. The constitutive behavior was modeled by defining the stress-strain points in the tensile test of the sheets.

The simulation was carried out in two steps. The first step simulated the indentation of the sheet metal using ABAQUS/Explicit code. Explicit code is better for simulating dynamic simulations. In this step, the bottom edge of the anvil was constrained from all the degrees of freedom. Also, the symmetric boundary conditions were applied to all the nodes on the axis. The reference point of the indenter was given a vertically downward displacement, and the resulting reaction on the indenter due to the penetration of the sheet metal was monitored. The second step simulated the springback of the sheet metal using ABAQUS/Standard code.

IV.2 Results of the simulation

Fig. 4.2 shows the equivalent plastic strain plot of the indentation on the 0.813mm thick Al3003-H14 sheet metal with a load of 100 kgf and an indenter of 1/8” diameter. It can be seen that at certain location, the sheet metal loses contact with the anvil after the indentation. Since the plastic strain is present throughout the thickness of sheet metal, and there is a permanent deformation on the bottom side of the sheet metal.

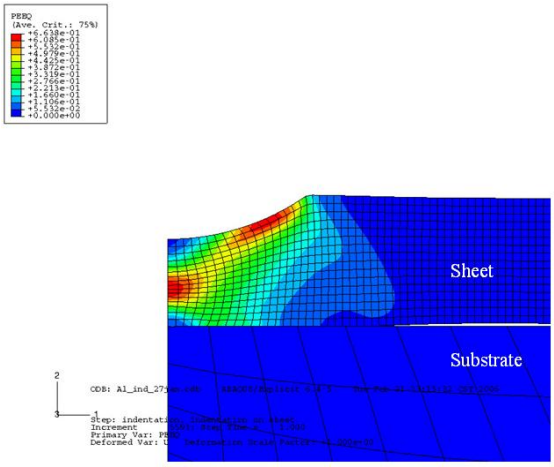

Fig. 4.2: Plastic strain plots of the indentation on 0.813 mm thick Al3003-H14 sheet metal

Although the plastic strain is not present in the anvil, as it can be seen in Fig 4.3, the stresses penetrate through the sheet metal and into the substrate. The stress distribution in the substrate is similar to the Hertz contact stresses.

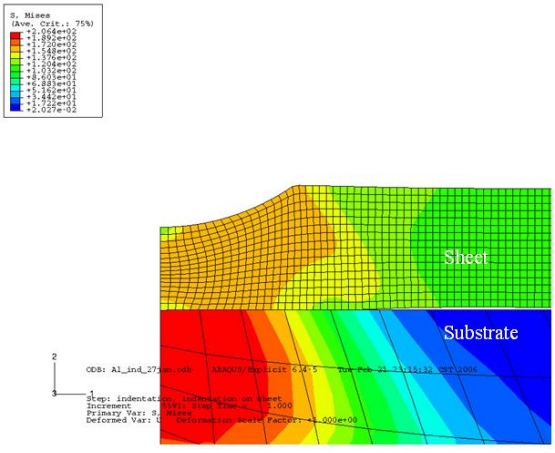

Fig. 4.3: Von mises stress plots of the indentation on the 0.813 mm thick Al3003-H14 sheet metal

The second step is the springback simulation in which the material recovers its elastic deformation after the indenter in unloaded. For this simulation, the details of the nodes and elements of the sheet metal obtained from the first step of the simulation were imported into the ABAQUS/Standard code by using the **IMPORT* option. Also, the state of the stresses and strains resulting from the first simulation for all the points was used as an initial condition for the second step by using the *STATE* and *UPDATE* options in the **IMPORT* command. As a result of this simulation, it was observed that the stresses in the sheet metal were relieved after the springback as seen in Fig. 4.4 and Fig. 4.5.

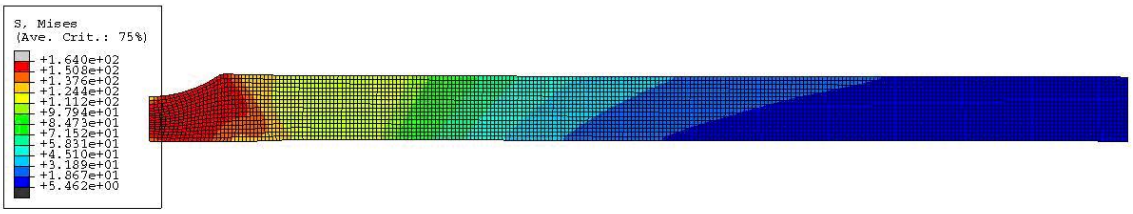

Fig. 4.4: Von mises stress plots of 0.813mm thick Al3003-H14 sheet metal before the springback

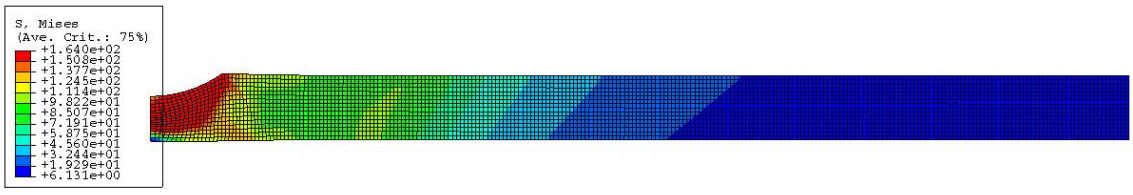

Fig. 4.5: Von mises stress plots of the 0.813mm thick Al3003-H14 sheet metal after the springback

It was also observed that the shape of the indentation changes after the springback. During this process of the elastic recovery, the nodes along the top surface of the sheet metal change their positions. This component of this movement along the horizontal direction is plotted in Fig. 4.6. The maximum value of this movement due to the springback was observed to be 0.002mm.

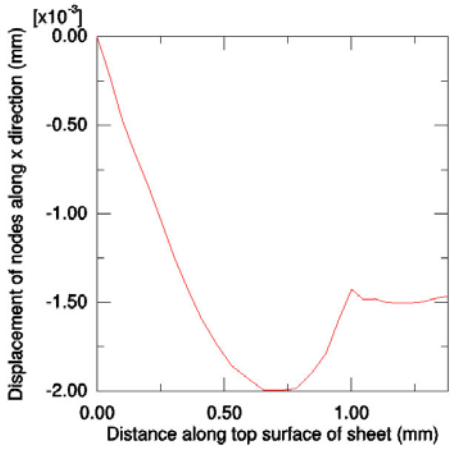

Fig. 4.6: Displacement of the nodes on sheet metal surface due to the springback

IV.3 Mesh refinement study

Initially, in order to select the best possible mesh for simulations, a mesh refinement study was carried out. In order to have better control over the mesh, a structured mesh was assigned for the sheet metal, whereas a biased mesh control, which arranges more nodes near the axis, was used for the anvil. The element of the *CAX4R* type was used for all the simulations.

Table 4.1 shows the different mesh configurations and output details for an indentation with a 10mm diameter indenter and a load of 500 kgf solved using the ABAQUS/Explicit solver. It can be seen from Fig. 4.7 that the computational time increased linearly with the density of the mesh. Out of the four meshes, the third mesh was chosen as the best one since the change in the radius of the indentation was not significant when the fourth mesh was selected, but the computational time increased significantly on its use.

Table 4.1: Details of the mesh refinement study

Mesh Number	Total number of elements	Total number of nodes	Smallest size of element (mm x mm)	Diameter of indentation (mm)	CPU Time (sec)
1	1350	1457	0.5 x 0.5	0.575	0.93
2	3750	3973	0.1 x 0.1	0.48269	1.63
3	11250	11618	0.05 x 0.05	0.46373	3.58
4	41250	41908	0.025 x 0.025	0.46377	11.78

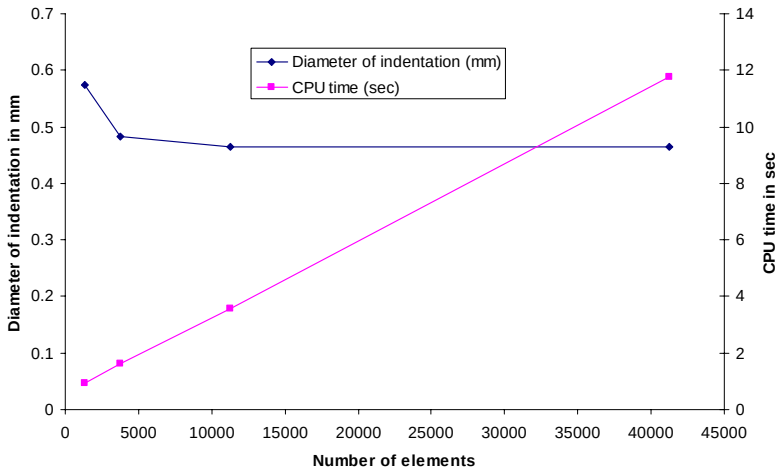

Fig. 4.7: The mesh refinement study

IV.4 Comparison of the Finite Element Analysis (FEA) results and the indentation experiments

The accuracy of the finite element method in predicting the indentation response is verified using the comparison between the applied indentation load in the experiments, and the reaction on the reference node used for the rigid indenter in the simulation. Table 4.2 shows the comparison of the experimental and FEA results for a spherical indentation on 0.813mm thick Al3003-H14 sheet metal with two different indenters. The same data is plotted in Fig. 4.8. Also, Table 4.3 shows the comparison of the experimental and FEA results for the spherical indentation on a 2.03mm thickness Al3003-H14 sheet metal with two different indenters.

Table 4.2: Experimental and FEA results for the indentation on a 0.813mm thick Al3003-H14 sheet metal

Indenter diameter (mm)	**Indentation load (N)**	**Depth of indentation (mm)**	**Reaction from FEA (N)**	**Depth of indentation from FEA (mm)**
3.175	441	0.1237	449	0.1242
3.175	588	0.1426	602	0.1459
3.175	981	0.2505	1032	0.2501
3.175	1471	0.4106	1543	0.4101
10	4905	0.5619	4968	0.5631

It can be observed from the data is plotted in Fig. 4.9 that the maximum applied indentation load is higher for the next case, since the sheet metal thickness is larger.

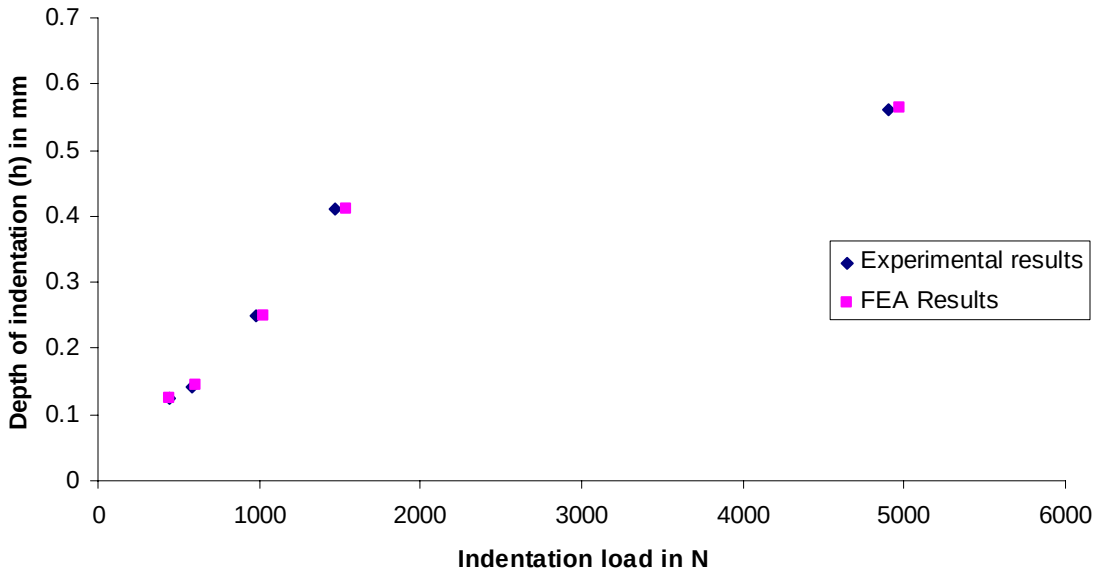

Fig. 4.8: Comparison of the spherical indentation experiment on 0.813mm thick Al3003-H14 sheet metal and the finite element simulation

Table 4.3: Experimental and FEA results for the indentation on a 2.03mm thick Al3003-H14 sheet metal

Indenter diameter (mm)	Indentation load (N)	Depth of indentation (mm)	Reaction from FEA (N)	Depth of indentation from FEA (mm)
3.175	441	0.123	432	0.1298
3.175	588	0.1396	600	0.1432
3.175	981	0.2405	979	0.2315
3.175	1471	0.3651	1507	0.3618
10	4905	0.411	4937	0.4278
10	9810	0.8941	10095	0.8851
10	14715	1.6299	14905	1.6305

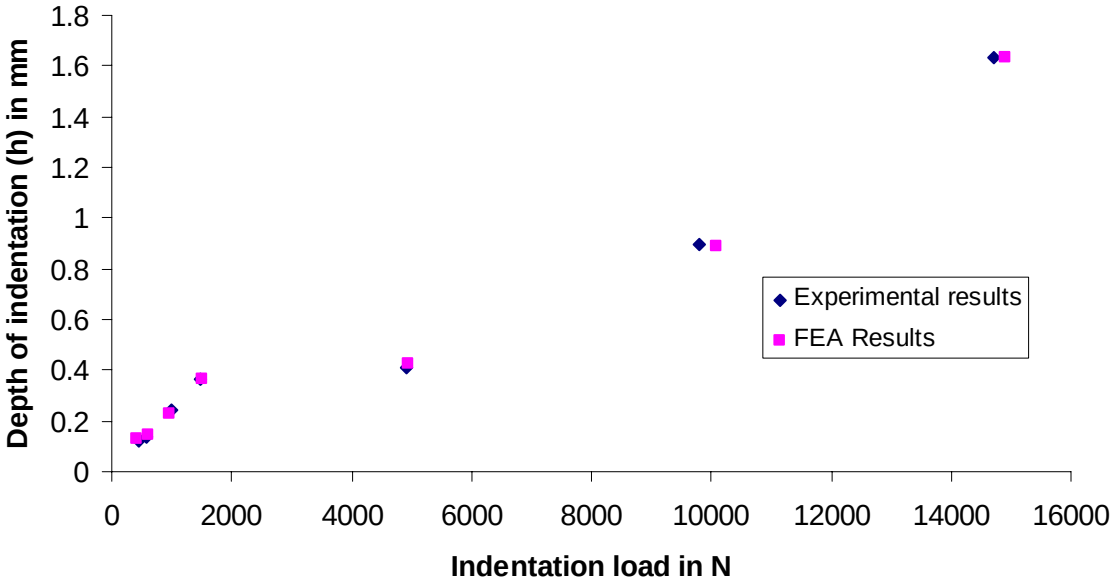

Fig. 4.9: Comparison of the spherical indentation experiment on a 2.03mm thickness Al3003-H14 sheet metal and the finite element simulation

From the above plots, it can be seen that the final results of the experiments and the simulations are in close agreement. This shows that the finite element method can predict accurately the indentation response of a material for the complex and highly non linear deformation process of indentation.

CHAPTER V

UNDERSTANDING THE ANVIL EFFECT

The process of the indentation on the thin sheets of metal was accurately simulated by the finite element method. To understand the anvil effect better, further study was conducted by repeating the simulations with changes of the appropriate parameter values in them.

V.1 Indentation parameters

As per the results noted in the previous chapters, it was inferred that the anvil effect is clearly dependent on the material and the thickness of the sheet metal. The constitutive behavior of the metal can be modeled with the power law equation that uses a strain hardening exponent n and a strain hardening constant K. An initial study was carried out by keeping the properties of the material constant, and varying the other parameters.

Three parameters for indentation were identified. The relation between the diameter of the indentation and the indentation load is governed by the pressure applied by the indenter. Two indentations made with different diameter indenters and loads can be compared based on the applied pressure as discussed in chapter two. Thus the indentation pressure was identified as the first indentation parameter. The thickness normalized to the radius of indenter was identified as the second parameter.

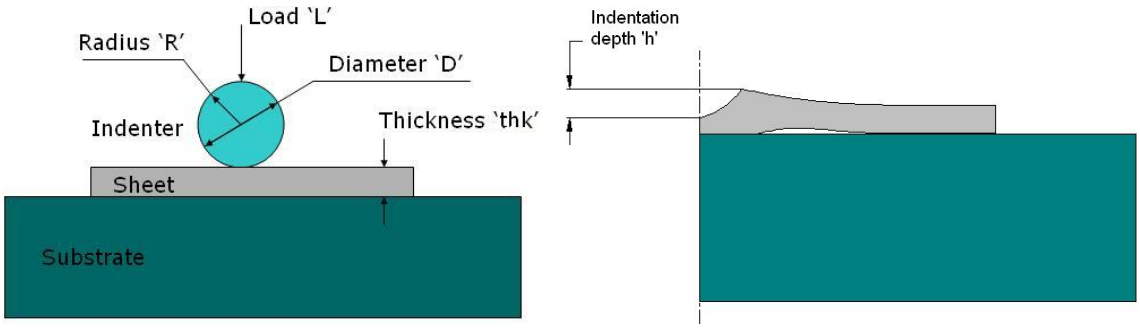

Fig. 5.1: Details of different indentation parameters

Finally, depth of indentation normalized to the radius of indenter was identified as the third parameter.

The three identified parameters are listed below, and their details are shown in Fig. 5.1.

- Indentation pressure: $P = L/D^2$
- Normalized thickness: thk/R
- Normalized depth of indentation: h/R

V.2 Anvil effect and the indentation pressure

Spherical indentations made with different indenters and different loads can be compared based on their respective indentation pressure. The data from indentation experiments carried out on Al3003-H14 and Al6061-T6 sheets of three different thicknesses was organized to analyze the variations. Fig. 5.2 and Fig. 5.3 show the

normalized depth plotted against the normalized thickness from the experiments conducted for the Al3003-H14 and Al6061-T6 sheet metals respectively.

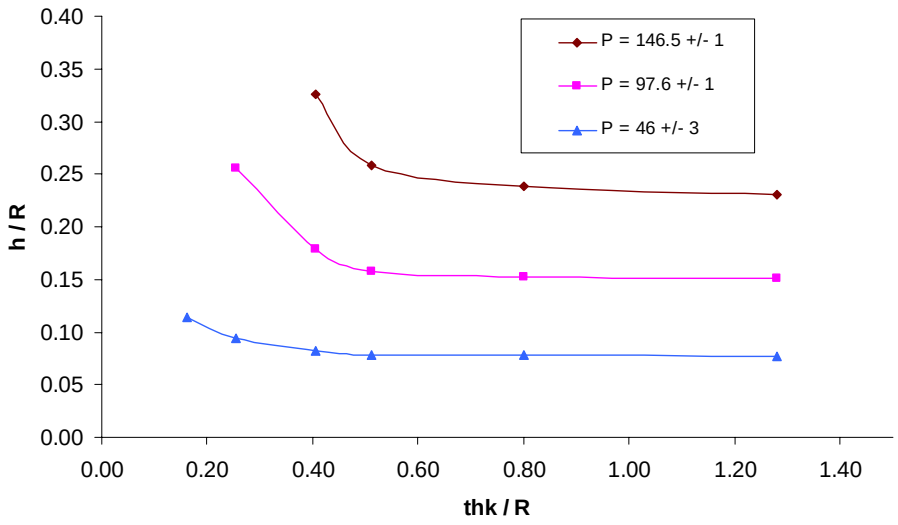

Fig. 5.2: Normalized depth vs thickness plots for the Al3003-H14 sheet metal

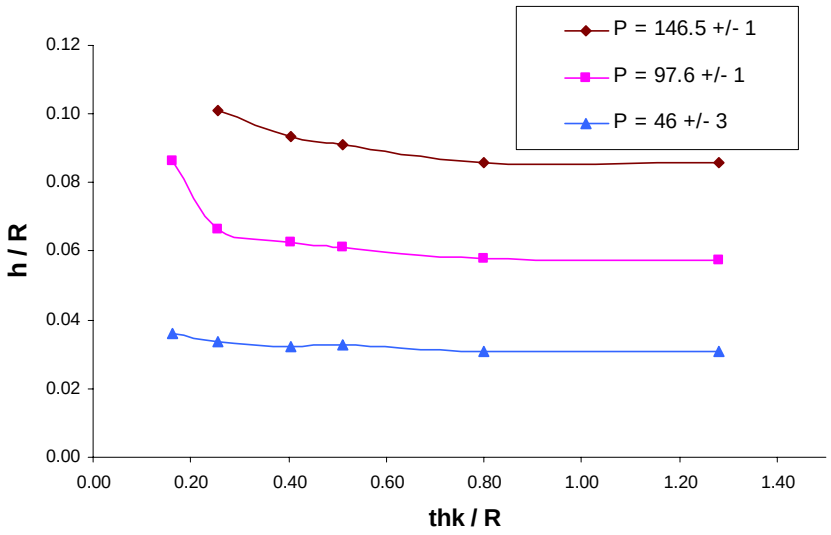

Fig. 5.3: Normalized depth vs thickness plots for the Al6061-T6 sheet metal

At higher indentation pressures, the depth of the indentation increases, which is reasonable. For larger thickness sheets, the depth of indentation is constant for the same indentation pressure indicating that there is no anvil effect. But when the thickness of sheet metal is reduced, the depth of the indentation goes on increasing instead of decreasing for the same indentation pressure. Intuitively, the resistance of a hard anvil to the indentation load should reduce the depth of the indentation; however, an exact reverse phenomenon was observed. For analyzing the reason behind such a response, a number of finite element simulations were conducted.

V.3 Anvil effect and the friction between the sheet metal and the anvil

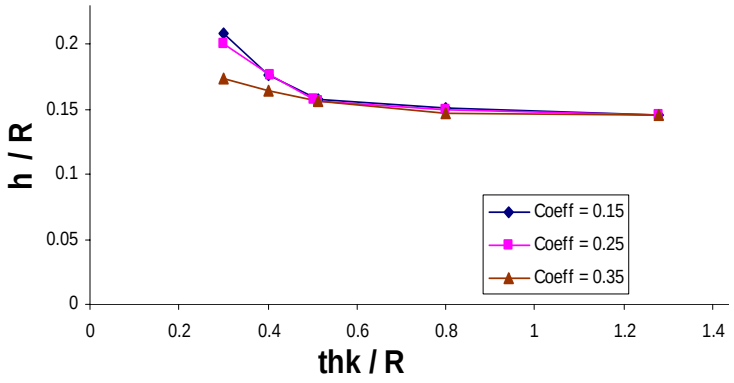

Fig. 5.4: Indentation response for three different values of the coefficients of friction between the Al3003-H14 sheet metal and the steel anvil

The value of the coefficient of friction used in the finite element simulations was obtained from experiments discussed in Section III.4. This value was varied in the simulation to study its effect on the response to the indentation. Fig 5.4 shows the result

of this study conducted for an indentation on the Al3003-H14 sheet metal of thickness 0.813 mm created using an indentation pressure of 100 MPa. It can be seen that when the thickness of the sheet metal is large enough as compared to the depth of the indentation, the coefficient of friction between the sheet metal and anvil does not affect the depth.

Thus it can be concluded that the friction between the sheet metal and the anvil plays an important role in the deformation, and the flow of the metal near the anvil, particularly for sheets having small thicknesses.

V.4 Anvil effect and work hardening

As seen in section V.2, it is known that the indentation response of a material depends on the indentation pressure. It also is observed that the anvil effect is different on the Al3003-H14 and Al6061-T6 sheet metals. In this section, results are noted for the study of the indentation response of the materials with different levels of work hardening conducted using finite element simulations.

The material definition for this finite element study mainly includes its mechanical properties obtained from the tensile test and its density. Simulations were conducted for different materials by altering these properties in the model. It is possible to conduct this

kind of study using simulations only and not using actual experiments, because producing metals having exact desired values of certain mechanical properties is almost impossible.

Fig. 5.5 shows the true stress – plastic strain curve used as the input for the simulations. As the value of the strain hardening exponent increases, the values of the stresses increase. The yield strength of all these materials was kept constant for all the simulations.

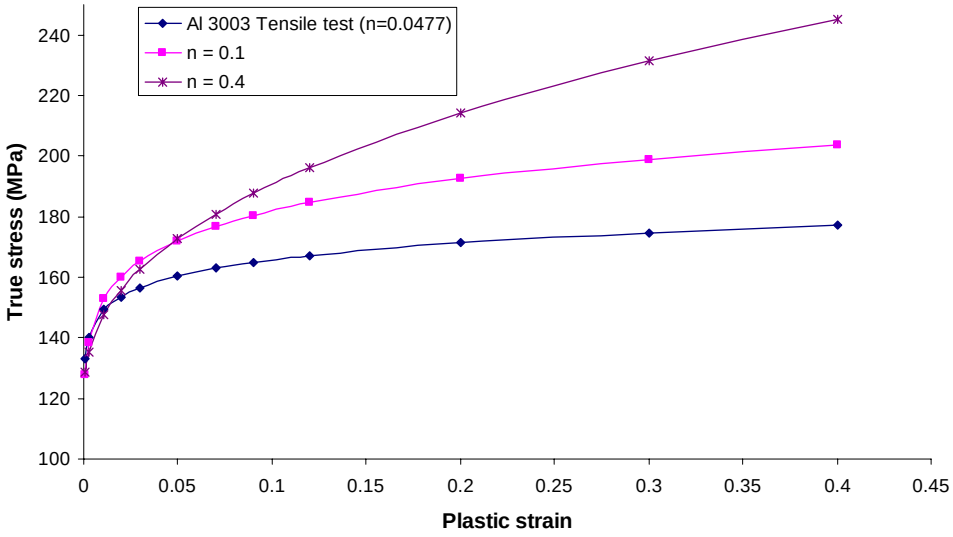

Fig. 5.5: Input data for the simulations of indentations on three metals with different work hardening histories

As it can be observed from the curve in Fig. 5.6, as the material becomes harder, the indentation depth goes on reducing.

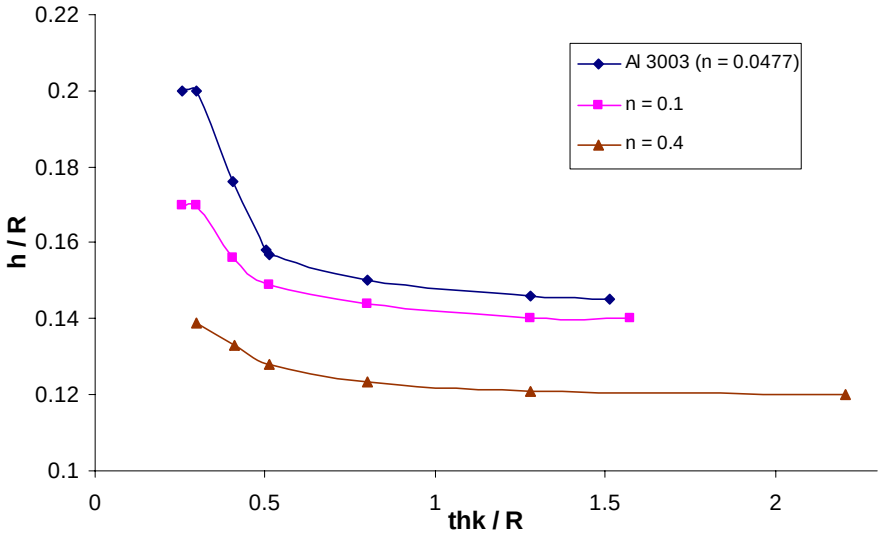

Fig. 5.6: Indentation response for the sheet metals with three different values of the strain hardening exponent

V.5 Anvil effect and the yield strength

Different materials can be incorporated into the finite element simulation by changing the input to the simulation in the form of the material properties. In the last section, the indentation response of the sheet metals with different work hardening histories but with the same yield strength was studied. In this section, the indentation response of the sheet metals with different yield strengths, but the same work hardening exponent is investigated. The input to the simulation given in the form of points on the tensile stress - strain curve for such metals is shown in Fig. 5.7. It can be seen from Figure that as the strength of the metal increases, its resistance to the indentation also increases.

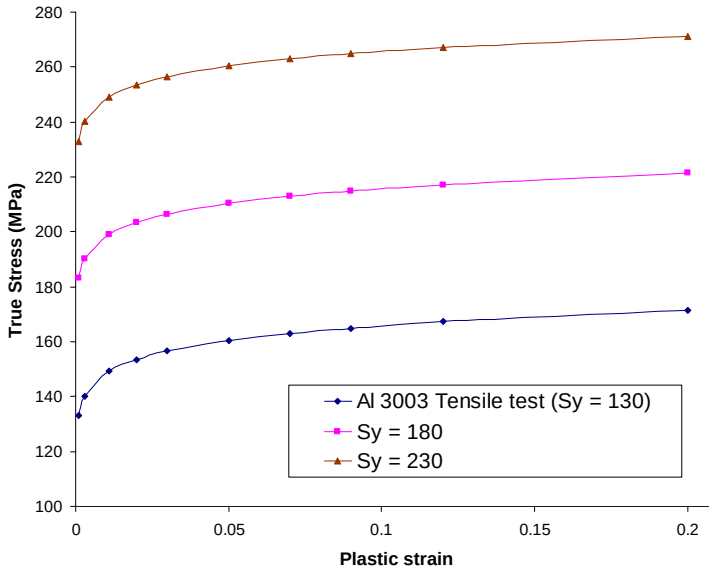

Fig. 5.7: Input data for the simulation of the three sheet metals with three different values of the yield strength

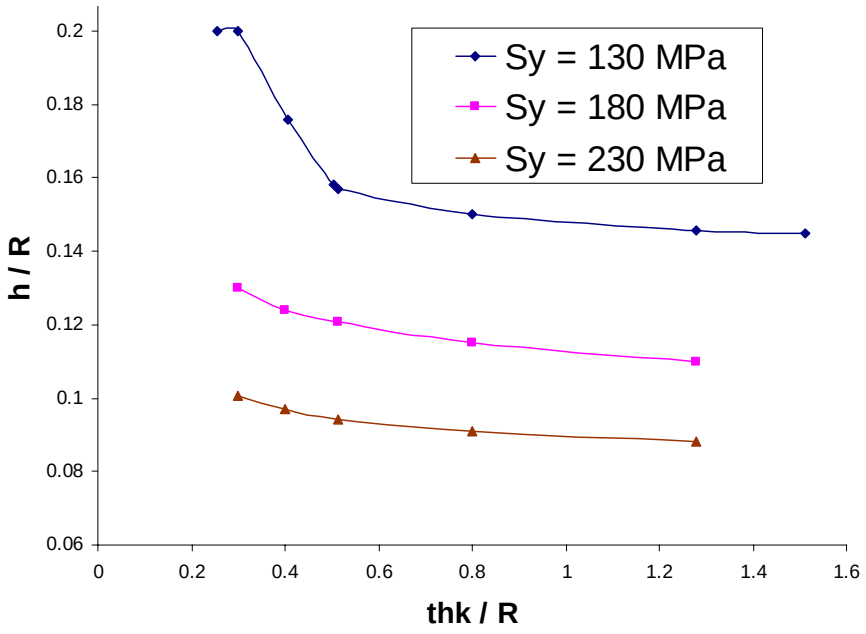

Fig. 5.8: Indentation response of the three sheet metals with three different values of the yield strength

Fig 5.8 shows the result of this study in the form of the normalized depth of indentation plotted against the normalized thickness. This curve in Figure shows that the depth of indentation decreases with the increasing yield strength of the material.

V.6 Modes of deformation during the indentation

The reason behind the response of metal sheets of different thicknesses to the indentation was analyzed using simulations and different cases of normalized thicknesses were studied for the same indentation pressure on the Al3003-H14 sheet metal, and they are described below.

Case 1) P = 98, thk/R = 1.51, h/R = 0.142

As seen in Fig 5.9, on indenting the 2.4mm thick Al3003-H14 sheet metal with a load of 100 kgf using an indenter of diameter of 1/8", it was observed that the indenter penetrates up to a depth of 0.757mm, at a normalized depth of 0.142. As apparent from Fig 5.9, the normal stresses in the direction of loading reached the bottom of the sheet metal after which the anvil started contributing in resisting the deformation in such a way that further reduction in the thickness of the sheet metal would only increase its contribution. The normal stresses in the radial direction are positive or tensile at the bottom of the sheet metal, whereas negative or compressive stresses are found at the top of the sheet metal, as shows in Fig. 5.10. Such tension-compression type stresses present

across the thickness of the sheet metal are similar to the bending mode of the deformation.

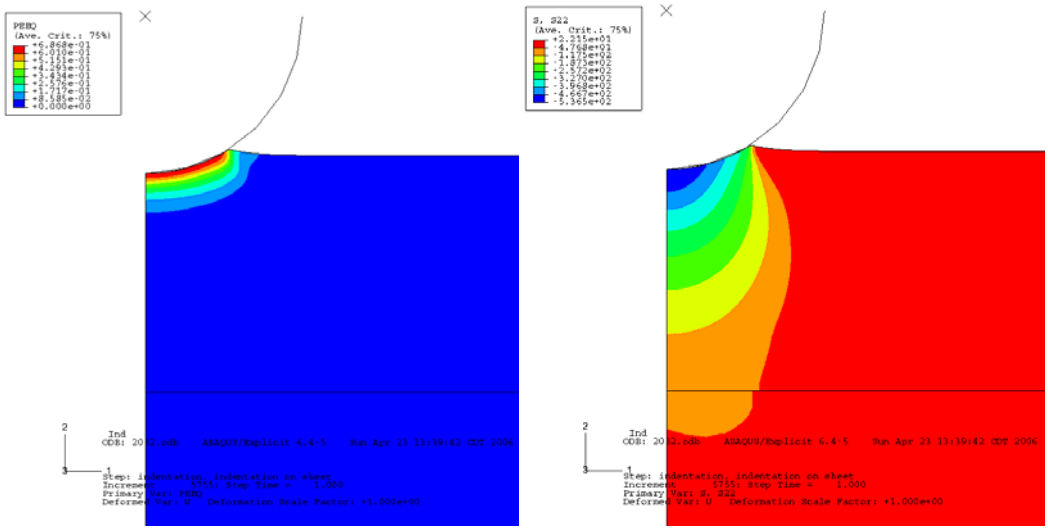

Fig. 5.9: Plastic strain contours for case 1 (left) and contours of the normal stresses in the axial direction for case 1(right)

Fig. 5.11 shows the variation of the radial stress along the nodes on the metal sheet which are centered in axial direction from top to bottom. Here, the normalized distance of zero represents the topmost node in the sheet metal along the axis. There is a gradient of about 400 MPa along the thickness of the sheet metal which indicates that, at that particular sheet metal thickness and load, the mode of deformation is not the indentation alone.

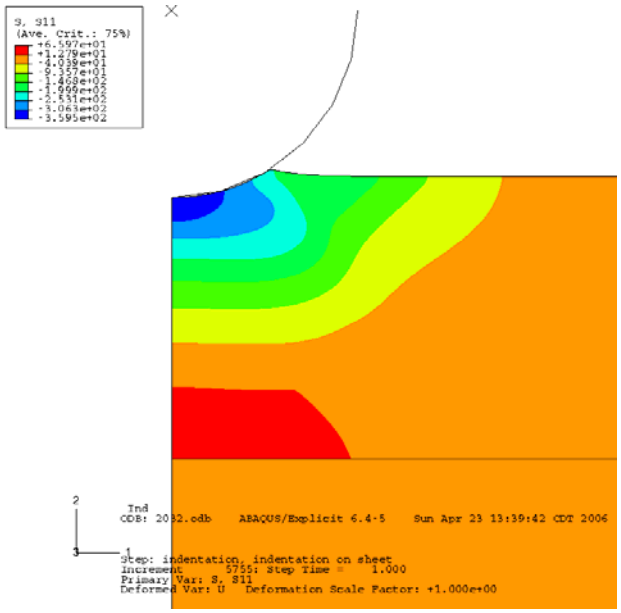

Fig. 5.10: Contours of the normal stresses in the radial direction for case 1

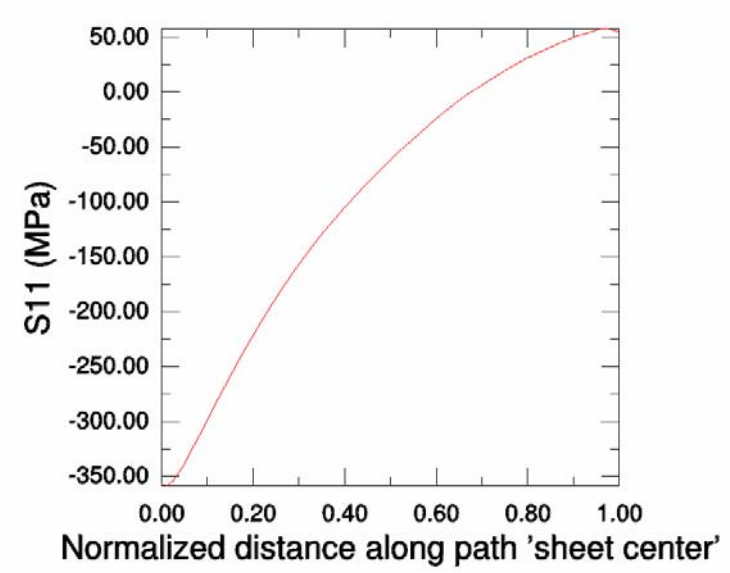

Fig. 5.11: Variation of the normal stresses in the radial direction along the sheet metal center for the Case 1

Case 2) P = 98, thk/R = 0.5, h/R = 0.158

When the thickness is reduced to 0.8 mm, the plastic strain contours reach the bottom of the sheet metal as seen in Fig. 5.12. Normal stresses in the axial direction are severely penetrated through the sheet metal and into the anvil as seen in Fig 5.13. The normal stresses in the axial direction along the nodes on the top surface of the anvil are plotted in Fig 5.14.

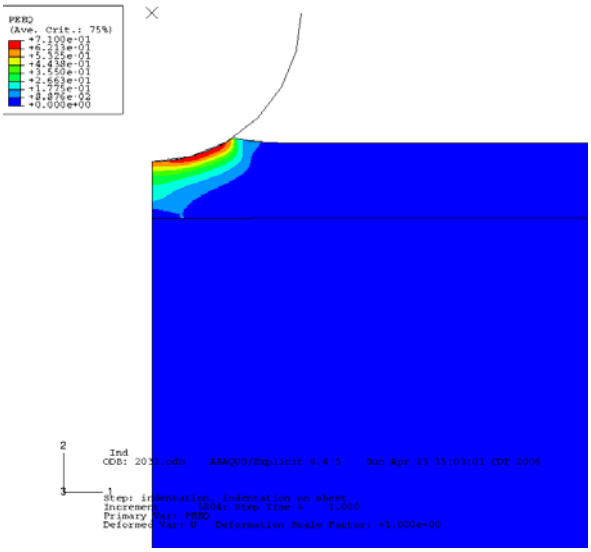

Fig. 5.12: Plastic strain contours for case 2

In this case, the magnitude of axial stresses is almost six times more than that in case 1 as seen in Fig. 5.14, indicating more contribution from the anvil in resisting the deformation.

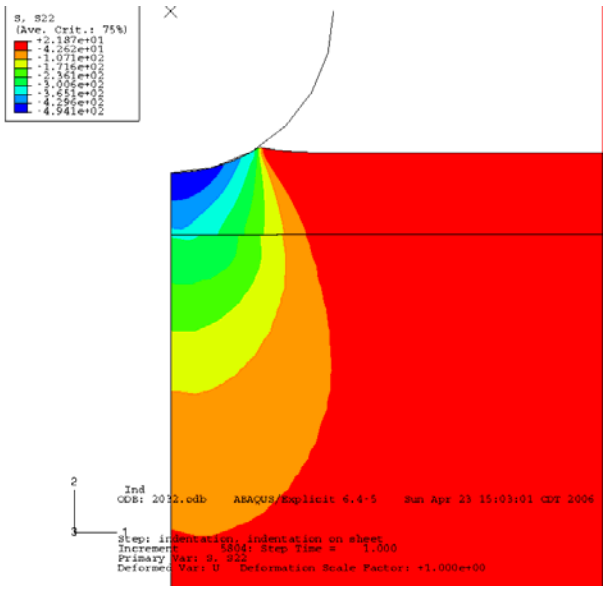

Fig. 5.13: Contours of the normal stresses in the axial direction for case 2

Fig 5.15 shows a normal radial stress plot in sheet metal and anvil. These stresses in the sheet metal right below the indenter are nearly the same as the previous case, whereas those near the bottom of the sheet metal become compressive.

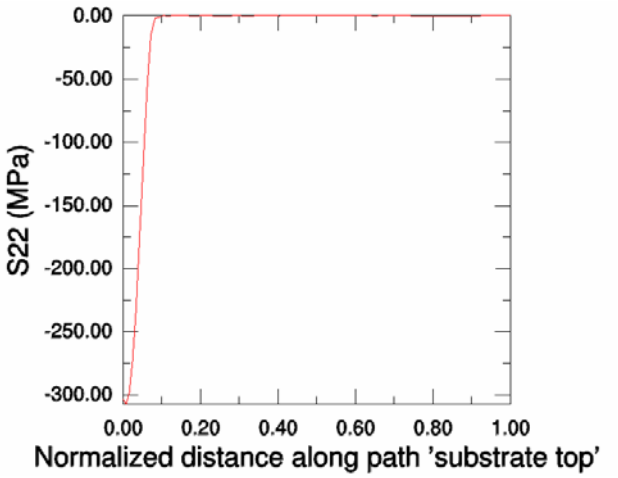

Fig. 5.14: Axial stress along the nodes on anvil top surface for case 2

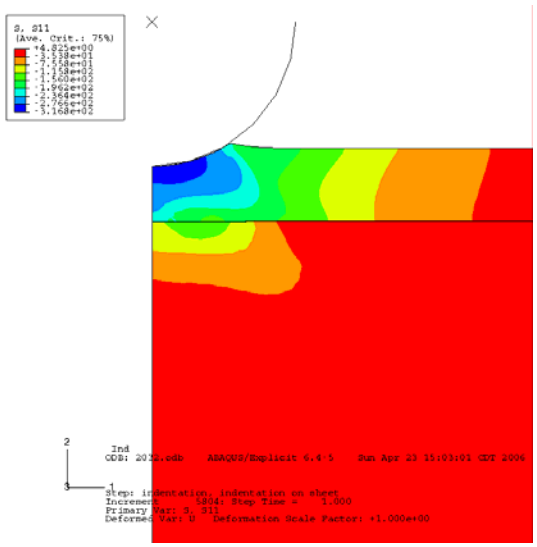

Fig. 5.15: Contours of the normal stresses in the radial direction for case 2

There is still a normal stress gradient of about 120 MPa in the sheet metal from top to bottom along the axis seen in Fig 5.16 as compared to 400 MPa in the last case.

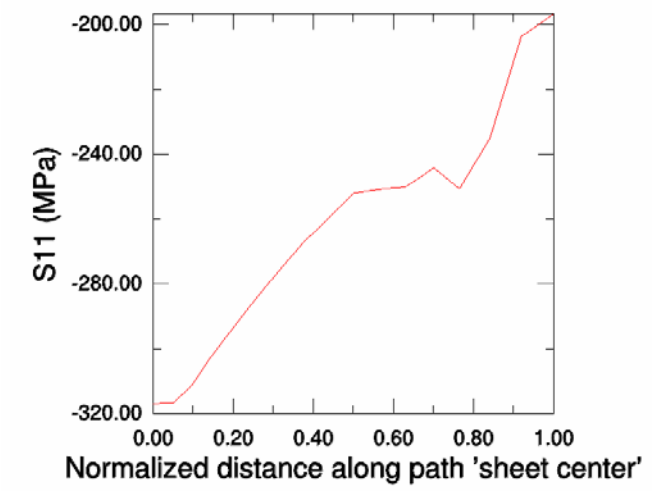

Fig. 5.16: Variation of the normal stress in the radial direction along the sheet metal center for case 2

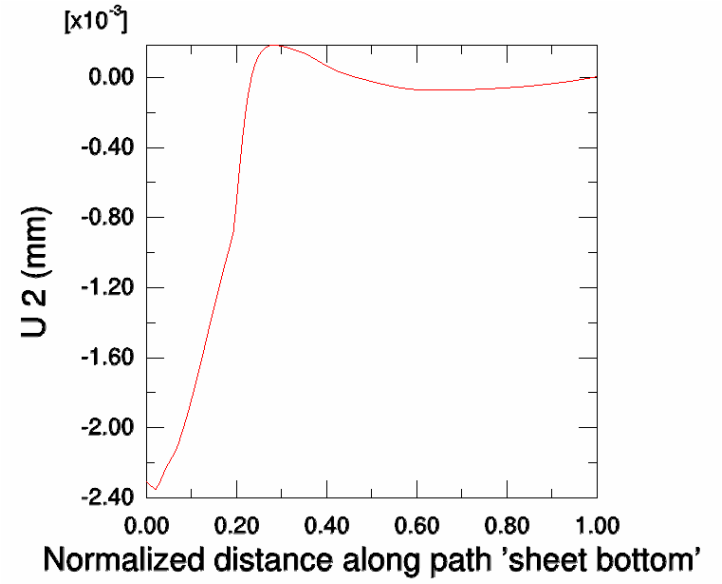

Fig. 5.17: Axial displacement of the nodes on bottom surface of the sheet metal for case 2

At this instance the sheet metal loses contact with the anvil as shown in Fig 5.17. Further reduction in the sheet metal thickness makes the sheet metal lift more. This provides additional depth of penetration.

Case 3) $L/D^2 = 100$, thk / R = 0.252, h /R = 0.2

When the thickness of sheet metal is further reduced to 1/4 of indenter radius, all the material below the indenter is plastically strained as shown in Fig 5.18. Contours of normal stresses in axial direction are shown in Fig 5.19. The sheet metal lifts due to the concentrated indentation load; however, this makes the anvil actively resist the deformation. Further reduction in thickness, does not increase height of indentation due

to the reaction from the anvil. Fig 5.20 shows the reaction from the anvil top surface in resisting the deformation which continues to grow.

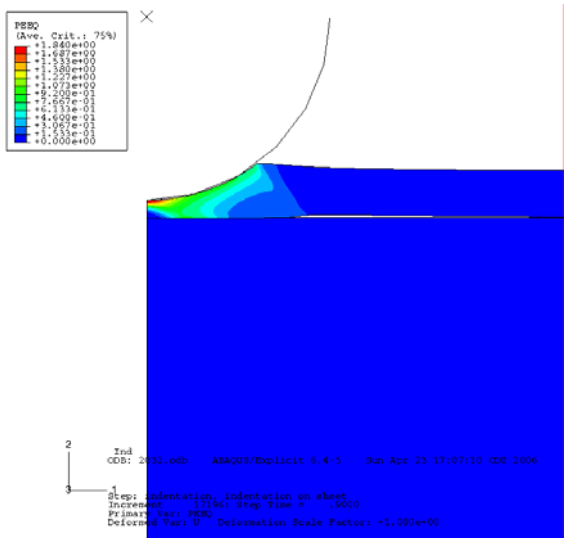

Fig. 5.18: Plastic strain contours for case 3

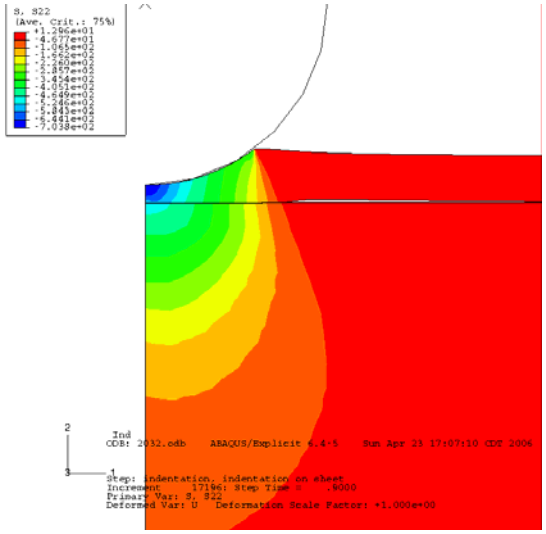

Fig. 5.19: Contours of the normal stresses in the axial direction for case 3

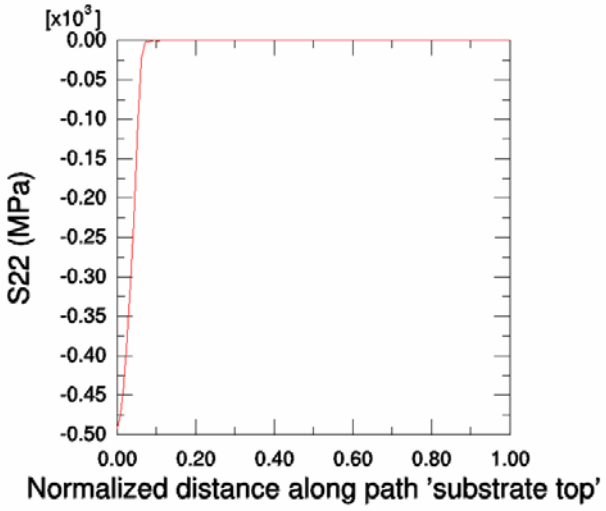

Fig. 5.20: Variation of the normal stress in the axial direction along the nodes on the top surface of the anvil for case 3

Case 4) L/D^2 = 100, thk / R = 0.157, h /R = 0.17

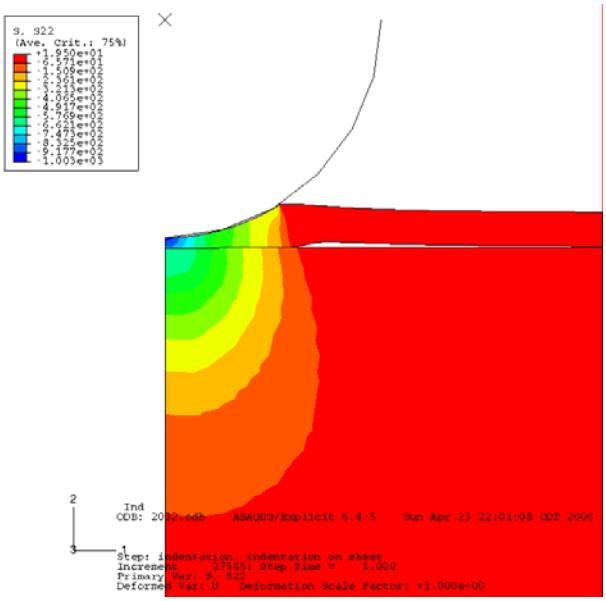

Fig. 5.21: Contours of the normal stresses in the axial direction for case 4

In this case the normalized thickness is reduced to 0.157. The depth of indentation reduces now instead of increasing. Fig 5.21 shows the normal stresses in loading direction. It can be seen that the stresses are almost continuous from sheet metal through anvil. There is still no plastic strain induced in the anvil, as seen in Fig. 5.22.

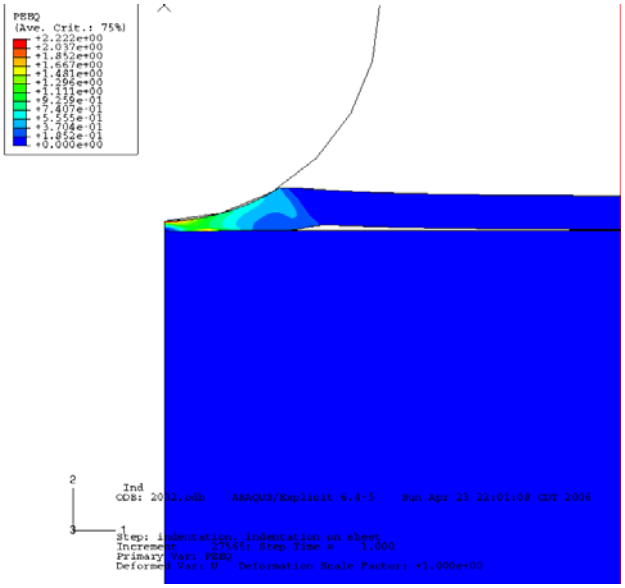

Fig. 5.22: Contours of plastic strain for case 4

To summarize, the response of the reduction in sheet metal thickness of metals at constant indentation pressure, is not purely indentation. It experiences bending mode followed by lifting of the sheet metal that leads to a forging mode of deformation.

V.7 Discussion

Different modes of deformation during the indentation with a sphere in normalized depth against normalized thickness can be separated as shown in Fig. 5.23 for Al3003-H14 and in Fig. 5.24 for Al6061-T6. All the lines of constant indentation pressure show a similar trend. For higher values of thickness relative to depth of indentation, the depth of indentation is constant. This indicates there is no anvil effect. As the normalized thickness approaches the 'one tenth rule', the normalized depths start increasing due to a combination of indentation and bending mode of deformation as seen in case 1.

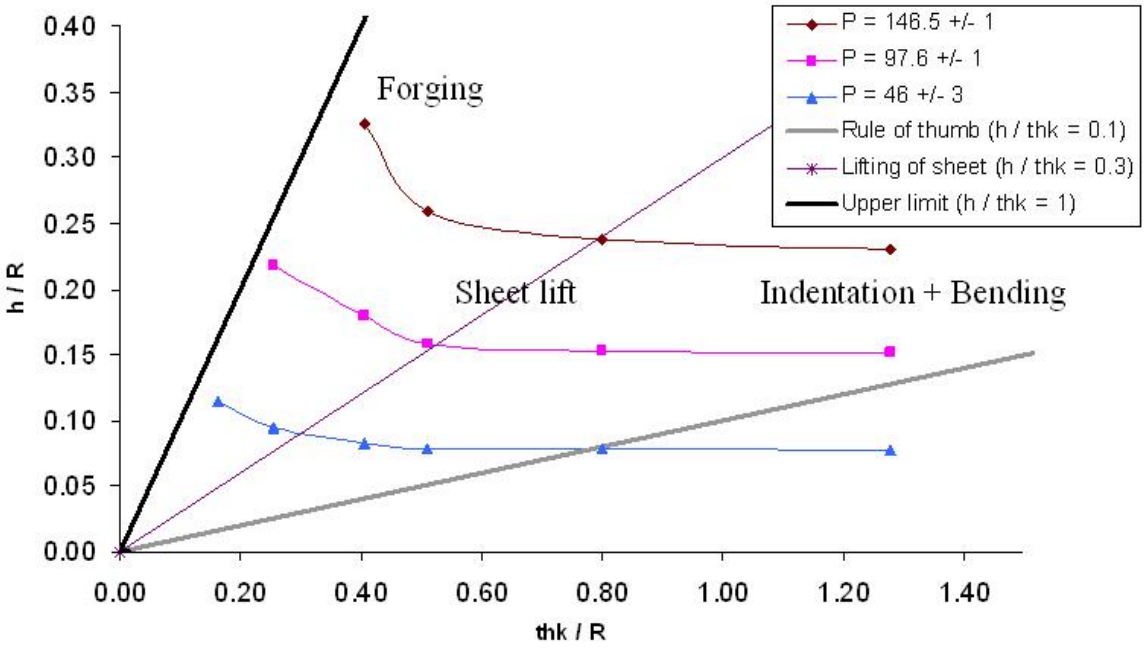

Fig. 5.23: Normalized depth vs thickness plots showing different deformation modes for Al3003-H14

Further reduction in thickness makes the sheet metal lose contact with the anvil as seen in case 2. This is seen at a penetration of about 30 % for Al3003-H14. Thereafter the indentation depth sharply increases as the material starts flowing in an outward radial direction. This is similar to the forging operation.

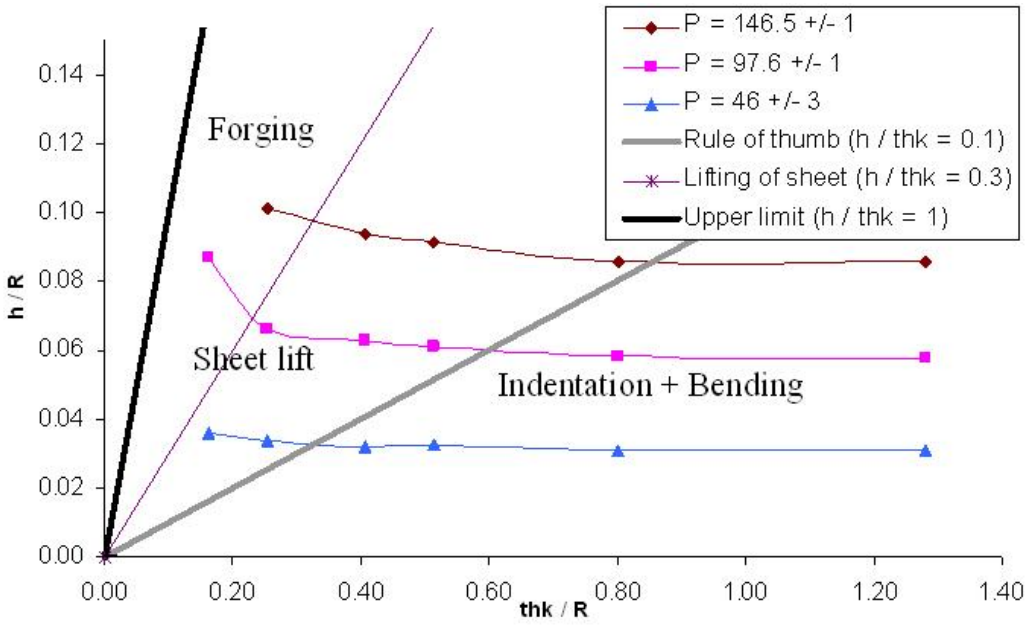

Fig. 5.24: Normalized depth vs thickness plots showing different deformation modes for Al6061-T6

CHAPTER VI

METHOD OF CORRECTION FOR THE ANVIL EFFECT

Normalized depth and thickness charts for Al3003-H14 and Al6061-T6 sheets show similar trend for constant indentation pressure. The anvil effect is seen clearly in these charts. The reason behind the increase in depth of indentation for smaller thickness sheets is justified by the change of deformation mode while indentation is occuring. The next step in this study was to quantify this anvil effect. This is also required in order to devise a method of correction for the anvil effect. With the help of this correction method, it is possible to carry out spherical indentation testing on the sheet metals, and correct the error introduced due to the anvil effect. One can then measure the depth of indentation on thin sheet metal, and obtain a depth of indentation 'equivalent' to the thick sheet metal of the same material by following the correction procedure.

VI.1 Curve fitting procedure

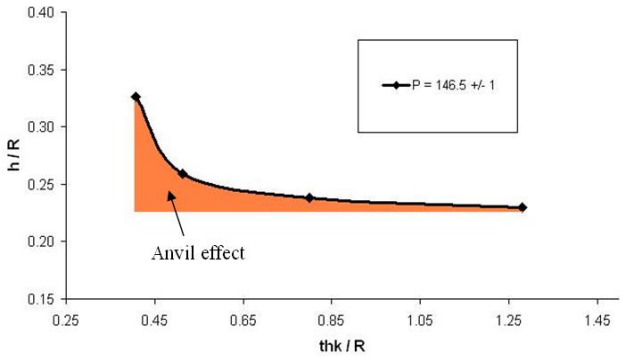

Fig. 6.1: Normalized depth vs thickness plots showing anvil effect on Al3003-H14

Curve fitting is the first step in quantifying the anvil effect. The nature of the curve for constant indentation pressure is as shown in Fig. 6.1. As the X coordinate (thk/R) decreases, the Y coordinate (h/R) on the curve increases. This type of curve can be fitted with functions such as an exponential function or with a second degree polynomial that has the product of X and Y coordinates as a constant.

In order to reproduce the exponential function, numerous points are required. This is not convenient since the method of correction is based on this function which will in turn require those many points on the curve. On the other hand, a second degree polynomial will need only three points for fitting. Therefore such a function was chosen for fitting a curve.

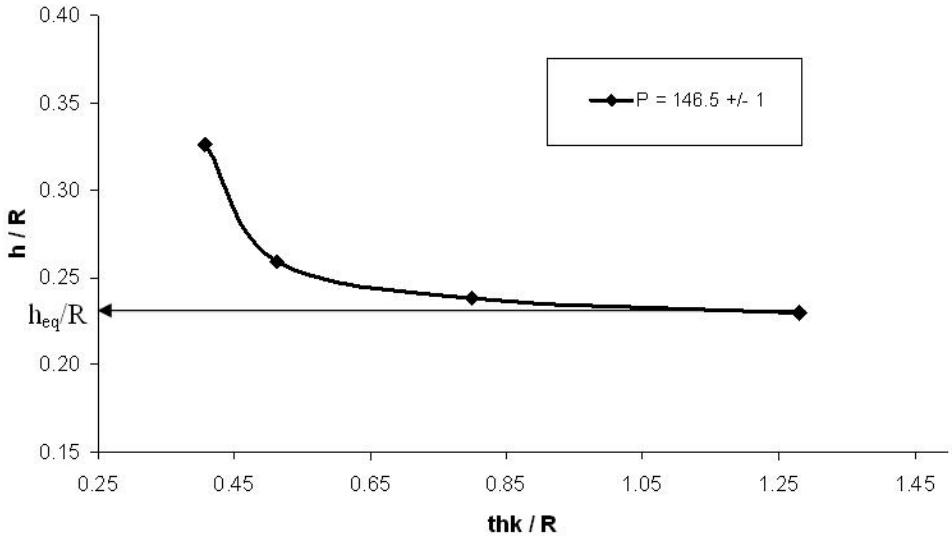

Fig. 6.2: Normalized depth vs thickness plots showing the equivalent depth of indentation on Al3003-H14

At higher values of normalized thickness, the depth of indentation remains the same. This is the depth of indentation without anvil effect. For all the points on the curve in Fig. 6.2, the normalized 'equivalent depth of indentation' is shown by arrow. This depth of indentation is for a particular indentation pressure. Equivalent depth of indentation was also considered as a parameter for curve fitting. The following equation was considered for curve fitting.

$$Y + d = \frac{a}{X - b} \tag{6-1}$$

where, $X = thk/R$,

$Y = h/R$,

$d = h_{eq}/R$.

The values of constants 'a' and 'b' are calculated for the best fitting curve through the data points. For this purpose, minimization of square of residual error technique was used. Residual error is the shortest distance between the data point and the point on the fitted curve. This error can be positive or negative depending on the relative location of the data point and curve; hence, the square of the residual errors is taken. Then the sum of squares is determined.

VI.2 Equations representing the anvil effect

The values of '*a*' and '*b*' for Al3003-H14 was calculated for different indentation pressures as listed in Table 6.1.

Table 6.1: Curve fitting parameters for Al3003-H14 sheet metal

Indentation pressure (N/mm^2)	***a***	***b***	h_{eq}/R
46	0.006	0.101	0.067
100	0.006	0.220	0.143
146	0.006	0.323	0.220

It is observed that the value of '*a*' remains the same for a material. The value of constant '*b*' is directly proportional to the indentation pressure. Experimental data and the fitted curve is plotted in Fig. 6.3.

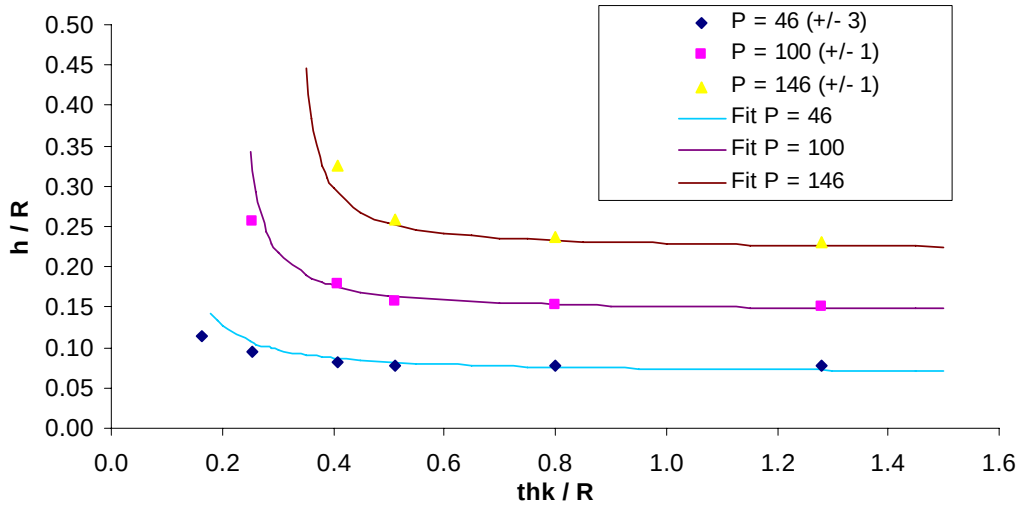

Fig. 6.3: Comparison of experiment data and fitted curve for Al3003-H14

Indentation pressure is also added in the equation to generalize the curve for any pressure by adding a new constant of proportionality '*c*'. Now the equation becomes,

$$\frac{h}{R}+\frac{h_{eq}}{R}=\frac{a}{\frac{thk}{R}-c\left(\frac{L}{D^2}\right)} \tag{6-2}$$

Rearranging this equation and substituting value of '*a*' and '*c*' for Al3003-H14, the equation (6-2)becomes,

$$h_{eq}=h-\frac{0.0060R}{\frac{thk}{R}-0.0022(P)} \tag{6-3}$$

Also, for Al6061-T6, the equation becomes,

$$h_{eq}=h-\frac{0.0025R}{\frac{thk}{R}-0.001(P)} \tag{6-4}$$

Here, the units of h_{eq}, h, thk, and R are mm and P is N/mm^2.

The anvil effect for any material can be quantified as,

$$\text{Anvil effect} = \frac{aR}{\frac{thk}{R} - c(P)} \tag{6-5}$$

The values of constants '*a*' and '*c*' need to be calculated. This can be obtained by using the method of correction explained in the next section.

VI.3 Procedure to obtain the equivalent geometry of indentation without the anvil effect

For a sheet metal with certain thickness, the anvil effect will change if the metal is changed. The anvil effect will depend on several factors associated with the metal such as its strength, work hardening history, and coefficient of friction with the anvil. Therefore, the values of constants '*a*' and '*c*' is unique for each sheet metal. Once we obtain these values, we can perform a spherical indentation test that shows the anvil effect and estimate the quantity of anvil effect using equation (6-5).

Following are the steps to be followed to obtain the values of '*a*' and '*c*':

1) Measure thickness of sheet metal in mm, and note it as 'thk'.

2) Carry our indentation test with loads and indenters mentioned in Table 6.2 or Table 6.3. Table 6.2 gives various load sets that can be used with the hardened steel ball indenters available in Rockwell and Brinell hardness testers. In Table 6.3, different indenter ball diameters are listed for standard indentation loads available in Rockwell and Brinell hardness testers.

Table 6.2: Different load sets for the standard indenters available

Indenter diameter (mm)	**Load set 1 (kg)**	**Load set 2 (kg)**	**Load set 3 (kg)**	**Load set 4 (kg)**
1.6	13	26	39	52
2.5	32	64	96	127
3.2	52	104	157	209
5.0	127	255	382	510
6.3	202	405	607	809
10.0	510	1019	1529	2039
12.7	822	1644	2466	3288
19.0	1840	3680	5520	7360
25.4	3288	6577	9865	13153

Table 6.3: Different set of indenters for the standard loads available

Indenter diameter (mm) set 1	**Indenter diameter (mm) set 2**	**Indenter diameter (mm) set 3**	**Indenter diameter (mm) set 4**	**Indentation Load (kg)**
1.72	1.21	0.99	0.86	15
2.43	1.72	1.40	1.21	30
2.97	2.10	1.72	1.49	45
3.43	2.43	1.98	1.72	60
4.43	3.13	2.56	2.21	100
5.42	3.84	3.13	2.71	150
9.90	7.00	5.72	4.95	500
14.01	9.90	8.09	7.00	1000
17.16	12.13	9.90	8.58	1500
24.26	17.16	14.01	12.13	3000

Any combination of indenters and loads from the four sets mentioned in Table 6.2 and Table 6.3 can be selected for the test. Each set is designed to produce the same value of indentation pressure; hence, two different sets should not be used. It is required to perform the test with three different loads and indenters from the selected set, since the curve is fitted with a function of second order polynomial. Moreover, at least two out of three readings should show anvil effect in the form of a mark on the sheet metal on the side facing the anvil and exactly below the indentation.

3) Note radius of indenter as 'R' in mm and load as 'L' in kgf.
4) Measure the height of indentation in mm and note it as 'h'.
5) Finally, use the MATLAB program given in Appendix C to obtain the values of equivalent height of indentation, '*a*' and '*c*'.

VI.4 Confirmation tests

The procedure given above was followed to obtain the values of different parameters for different materials. The curve was fitted using those parameters for one value of indentation pressure. Then for verification, those parameters were used to plot the curve at different indentation pressure. The experiments were carried out at that pressure on the same sheet metal. The predictions from the curve fitting model agree with the experimental results as seen in Fig. 6.4, Fig. 6.5, Fig. 6.6 and Fig. 6.7.

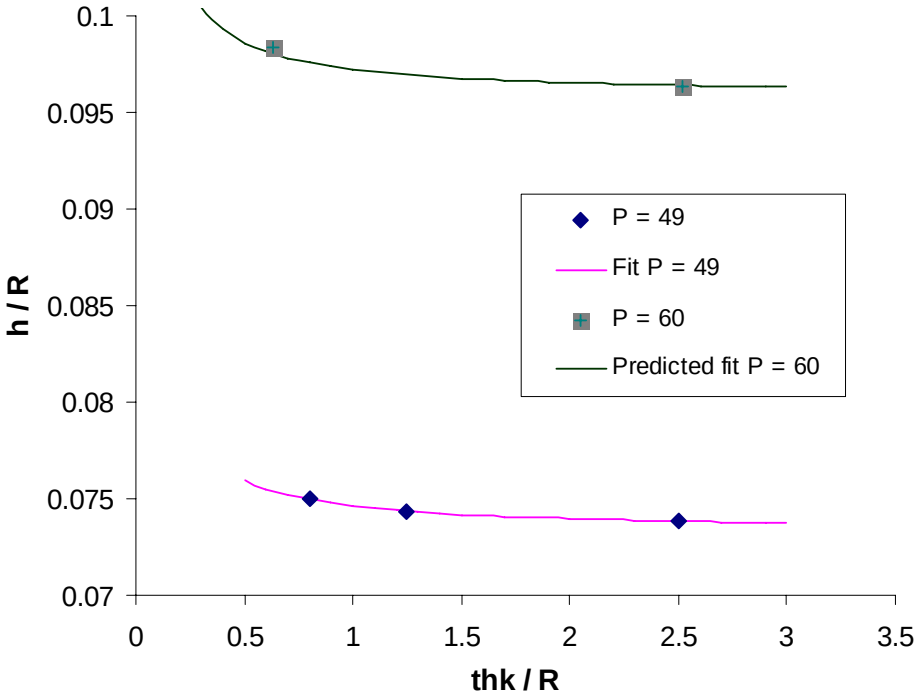

Fig. 6.4: Confirmation test on 4 mm thick commercial Niobium

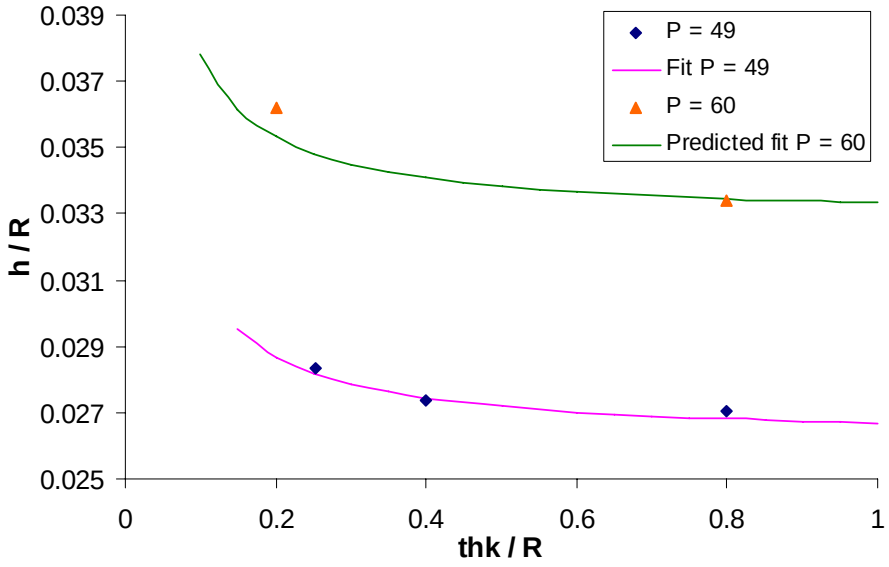

Fig. 6.5: Confirmation test on 1.27 mm thick Al2024-T3

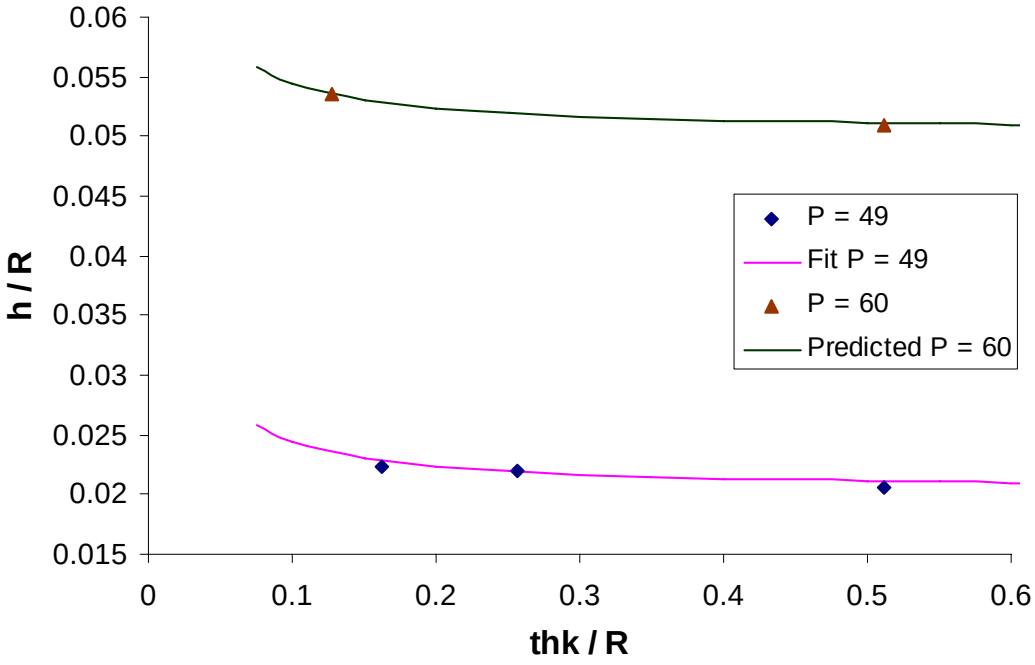

Fig. 6.6: Confirmation test on 0.813 mm thick Al7075-T6

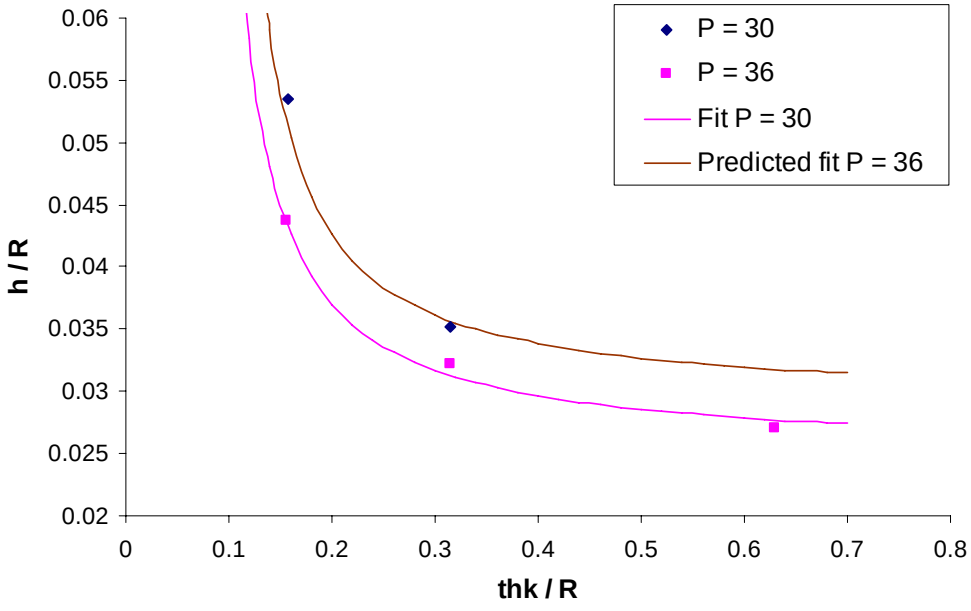

Fig. 6.7: Confirmation test on 0.5 mm thick 1020 low carbon steel

VI.5 Useful range for the method of correction of the anvil effect

The proposed method of prediction of the equivalent depth of indentation without the anvil effect was verified for different sheet metals of different thicknesses. It shows good agreement between the experimental results and the curve fitting model. The method of correction requires the spherical indentation test to be carried out with at least three different indenters, and corresponding loads for obtaining all the curve fitting parameters for a sheet metal. If these three tests do not show anvil effect in the form of mark or dent on the back side of sheet metal, then it will not be possible to obtain curve fitting parameters. Thus, if the depth of indentation very small compared to the thickness of the sheet metal then there are less chances of presence of the anvil effect. On the other hand, if the depth of indentation is close to the thickness of the sheet metal, or the anvil effect is very severe, then it becomes difficult to measure the depth of indentation accurately. If measurements at such a high deformation is used for obtaining the curve fitting parameters, then the curve fitting model becomes less accurate. It is observed that the difference between the curve fitting model, and the experimental readings starts to become significant when the depth of indentation reaches 80% of the thickness of the sheet.

Thus, for the ratio of depth of indentation to the thickness of the sheet metal, a lower limit of 0.1 and an upper limit of 0.8 should be followed as the useful range for the method of correction of the anvil effect.

CHAPTER VII

SUMMARY AND CONCLUSIONS

Spherical indentation testing has many applications such as hardness evaluation, extraction of tensile test properties, and finding out process parameters. Anvil effect introduces an error in spherical indentation testing. This effect can be identified in the form of a mark or dent on the backside of the sheet metal due to spherical indentation test. With the conventional methods such as Brinell and Rockwell hardness testing and with their available standard loads, it is difficult to avoid anvil effect while dealing with sheet metals. This anvil effect in the form of a mark was identified when Al3003-H14 and Al6061-T6 sheets of different thickness were tested on the steel anvils. If the thickness of the sheet metal is reduced, and the indentation test is carried out on it, then the penetration depth goes on increasing instead of decreasing for constant indentation pressures. The reason behind this was a change in mode of deformation. When the thickness of the sheet metal is reduced, and the indentation test is carried out on it, then the sheet metal experiences first indentation, then bending followed by lifting which leads to forging mode of deformation. This was identified using a finite element simulation of indentation process.

Further investigation was carried out using parameter variation in simulation and experiments. Parametric charts were plotted, and a second order polynomial curve was fitted through the data points. The equation of this curve gives quantification for anvil

effect. Anvil effect was identified as a function of thickness of sheet metal, indenter radius, indentation load, and two different material constants.

A method to correct this anvil effect was also developed using the equations representing the anvil effect. This method can be used to determine the equivalent geometry of indentation without the anvil effect. In other words, the limitation of spherical indentation testing due to the thickness of sheet metal is improved. Essentially, this procedure gives parameters defining the curve for anvil effect. A MATLAB program was developed for this purpose. Indentation testing on a sheet metal using three different indenters and corresponding loads is required for this method. For accurately predicting equivalent depth of indentation, a lower limit of 10 % and an upper limit of 80 % for penetration depth (ratio of depth of indentation and thickness of sheet metal) was identified. Confirmation tests were carried out on commercially available Niobium, Al 2024-T3, Al7075-T6, and 1020 low carbon steel sheets. These tests show good agreement between fit, prediction, and experiments for anvil effect.

REFERENCES

1. Edmund Isakov, 2000, *Mechanical Properties of Work Materials,* Hanser Gardner Publications, Cincinnati, OH
2. ASTM, 2000. Annual Book of ASTM Standards. **03.01**.
3. Lysaght V. E., 1949, *Indentation Hardness Testing*, Reinhold Publishing Corporation, New York, NY.
4. Voort Vander, 1984, *Metallography Principles and Practice,* Material Science and Engineering Series, McGraw-Hill, Inc., New York, NY.
5. Tabor, D., 1951, *The Hardness of Metals*, Oxford University press, London.
6. Atkins A.G., and Tabor D., "Plastic indentation of metals with cones", *Journal of Mechanics and Physics of Solids*, **13**, 1965, pp. 149-164.
7. Kenyon R. L., 1934, "Effect of Thickness on the Accuracy of Rockwell Hardness Tests on Thin Sheets", *Proc. American Society for Testing Materials*, 34, II.
8. Heyer R. H., 1937, " Analysis of Brinell Hardness Test", *Proc. American Society for Testing Materials*, 37, II.
9. Waters N. E., 1965, "The indentation of thin rubber sheets by spherical indentors", *Brit. Journal of Applied Physics*, **16**, pp. 557-563.
10. Lebouvier D., Gilormini P., Felder E., 1985, "A kinematic solution for plane-strain indentation of a bi-layer", *Journal of Physics*, **18**, pp. 199-210.

11. Taylor D. J., Kragh A. M., "Determination of the rigidity modulus of thin soft coatings by indentation measurements," *Journal of Physics D: Applied Physics*, **3**, pp. 29-32.
12. Pitts E., 1970, "The indentation of elastic layers," *Journal of Physics D: Applied Physics*, **3 (12)**, pp. 1803-1810.
13. Yang Fuqian, 2003, "Axisymmetric indentation of an incompressible elastic thin film," *Journal of Physics D: Applied Physics*, **36**, pp. 50-55.
14. Yo-Han Yoo, Woong Lee, Hyunho Shin, 2003, "Effect of work hardening on the critical indentation limit in spherical nano-indentation of thin film / anvil systems", *Surface and Coatings Technology,* **179**, pp. 324-332.
15. Panich N., Sun Y., 2003, "Effect of penetration depth on indentation response of soft coatings on hard anvils: a finite element analysis," *Surface and Coatings Technology*, **182**, pp. 342-350.
16. Chaiwut Gamonpilas, Esteban P. Busso, 2004, "On the effect of anvil properties on the indentation behaviour of coated systems," *Materials Science and Engineering A*, **380**, pp. 52-61.
17. Sridhar I., Zheng Z. W., Johnson K. L., 2004, "A detailed analysis of adhesion mechanics between a compliant elastic coating and a spherical probe," *Journal of Physics D: Applied Physics*, **37**, pp. 2886-2895.
18. *ABAQUS User's Manual*, version 6.4, Abaqus Inc., 2006.

APPENDIX A

INPUT FILE FOR THE FIRST STEP (PROCESS OF SPHERICAL INDENTATION) OF FINITE ELEMENT SIMULATION USING ABAQUS/EXPLICIT

```
*Heading
 Ind
** Job name: 2032 Model name: Model-1
*Preprint, echo=NO, model=NO, history=NO, contact=NO
** ----------------------------------------------------------------
**
** PART INSTANCE: indenter-1
**
*Surface, type=SEGMENTS, name=indenter-1_indenter
START,       1.5875,       1.5875
 CIRCL,          0.,          0.,          0.,       1.5875
** ----------------------------------------------------------------
**
** PART INSTANCE: sheet-1
**
*Node
      1,          0.,           0.
      2,          0.,       -0.025
      3,          0.,        -0.05
      4,          0.,       -0.075
      5,          0.,        -0.1
           .
           .
           .
   8513,        12.5,         -0.3
   8514,        12.5,       -0.325
   8515,        12.5,        -0.35
   8516,        12.5,       -0.375
   8517,        12.5,         -0.4
*Element, type=CAX4R
  1,    1,    2,   19,   18
  2,    2,    3,   20,   19
  3,    3,    4,   21,   20
```

```
  4,   4,   5,  22,  21
  5,   5,   6,  23,  22
  .
  .
  .
7995, 8494, 8495, 8512, 8511
7996, 8495, 8496, 8513, 8512
7997, 8496, 8497, 8514, 8513
7998, 8497, 8498, 8515, 8514
7999, 8498, 8499, 8516, 8515
8000, 8499, 8500, 8517, 8516
** Region: (sheet:Picked)
*Elset, elset=sheet-1__PickedSet3, generate
   1,  8000,     1
** Section: sheet
*Solid Section, elset=sheet-1__PickedSet3, material=AL-Sheet
1.,
** ----------------------------------------------------------------
**
** PART INSTANCE: anvil-1
**
*Node
  8518,          0.,        -10.
  8519,     0.368118,        -10.
  8520,    0.7357206,        -10.
  8521,     1.103093,        -10.
  8522,     1.470417,        -10.
        .
        .
        .
  9838,     16.24405,        -0.4
  9839,     16.94672,        -0.4
  9840,     17.67285,        -0.4
  9841,     18.42323,        -0.4
  9842,     19.19867,        -0.4
  9843,          20.,        -0.4
*Element, type=CAX4R
8001, 8518, 8519, 8570, 8569
8002, 8519, 8520, 8571, 8570
8003, 8520, 8521, 8572, 8571
8004, 8521, 8522, 8573, 8572
      .
      .
      .
```

```
9246, 9787, 9788, 9839, 9838
9247, 9788, 9789, 9840, 9839
9248, 9789, 9790, 9841, 9840
9249, 9790, 9791, 9842, 9841
9250, 9791, 9792, 9843, 9842
** Region: (anvil:Picked)
*Elset, elset=anvil-1__PickedSet2, generate
 8001,  9250,     1
** Section: anvil
*Solid Section, elset=anvil-1__PickedSet2, material=Anvil-Steel
1.,
*System
*Node
   9844,          0.,       1.5875,          0.
*Nset, nset=indenter_reference
9844,
*Nset, nset=sht_cen, generate
  1,  17,   1
*Elset, elset=sht_cen, generate
  1,  16,   1
*Nset, nset=sht_left_bot
 17,
*Nset, nset=sht_right_bot
 8517,
*Nset, nset=sub_cen, generate
 8518,  9793,    51
*Elset, elset=sub_cen, generate
 8001,  9201,    50
*Nset, nset=sub_bot, generate
8518, 8568,   1
*Elset, elset=sub_bot, generate
8001, 8050,   1
*Elset, elset=_sht_bot_S2, generate
   16,  8000,    16
*Surface, type=ELEMENT, name=sht_bot
_sht_bot_S2, S2
*Elset, elset=_sht_top_S4, generate
    1,  7985,    16
*Surface, type=ELEMENT, name=sht_top
_sht_top_S4, S4
*Elset, elset=_sub_top_S3, generate
 9201,  9250,     1
*Surface, type=ELEMENT, name=sub_top
_sub_top_S3, S3
```

```
** Constraint: rigid_indenter
*Rigid Body, ref node=indenter_reference, analytical surface=indenter-1_indenter,
position=CENTER OF MASS
*Amplitude, name=”indenter disp”, definition=SMOOTH STEP
0., 0., 1., -0.25
**
** MATERIALS
**
*Material, name=AL-Sheet
*Density
 2.7,
*Elastic
70000.0, 0.35
*Plastic
 130.0, 0.0
 140.2, 0.003
 149.2, 0.011
 153.5, 0.02
 156.5, 0.03
 160.4, 0.05
 163.0, 0.07
 164.9, 0.09
 167.2, 0.12
*Material, name=Anvil-Steel
*Density
 7.8,
*Elastic
210000., 0.3
*Plastic
207.,  0.
450., 0.1
**
** INTERACTION PROPERTIES
**
*Surface Interaction, name=”friction indenter and sheet”
*Friction
0.,
*Surface Interaction, name=”friction sheet and anvil”
*Friction
 0.25,
**
** BOUNDARY CONDITIONS
**
** Name: indenter_rp Type: Symmetry/Antisymmetry/Encastre
```

```
*Boundary
indenter_reference, XSYMM
** Name: sheet_cen Type: Symmetry/Antisymmetry/Encastre
*Boundary
sht_cen, XSYMM
** Name: anvil_bot Type: Symmetry/Antisymmetry/Encastre
*Boundary
sub_bot, ENCASTRE
** Name: anvil_cen Type: Symmetry/Antisymmetry/Encastre
*Boundary
sub_cen, XSYMM
** ----------------------------------------------------------------
**
** STEP: indentation
**
*Step, name=indentation
indentation on sheet
*Dynamic, Explicit
, 1.
*Bulk Viscosity
0.06, 1.2
**
** BOUNDARY CONDITIONS
**
** Name: indenter disp Type: Displacement/Rotation
*Boundary, amplitude="indenter disp"
indenter_reference, 2, 2, 1.
**
** INTERACTIONS
**
** Interaction: indenter and sheet
*Contact Pair, interaction="friction indenter and sheet", mechanical
constraint=KINEMATIC, cpset=indenter and sheet
sht_top, indenter-1_indenter
** Interaction: sheet and anvil
*Contact Pair, interaction="friction sheet and anvil", mechanical
constraint=KINEMATIC, cpset=sheet and anvil
sub_top, sht_bot
**
** OUTPUT REQUESTS
**
*Restart, write, number interval=1, time marks=NO
**
** FIELD OUTPUT: F-Output-1
```

```
**
*Output, field, variable=PRESELECT
**
** FIELD OUTPUT: F-Output-2
**
*Output, field
*Node Output, nset=indenter_reference
RF, U, V
**
** HISTORY OUTPUT: H-Output-1
**
*Output, history, variable=PRESELECT
**
** HISTORY OUTPUT: H-Output-2
**
*Output, history
*Node Output, nset=indenter_reference
RF2, U2
*End Step
```

APPENDIX B

INPUT FILE FOR THE SECOND STEP (SPRINGBACK) OF FINITE ELEMENT SIMULATION USING ABAQUS/STANDARD

```
*HEADING
*IMPORT,STEP=1,INT=1,STATE=YES, UPDATE=YES
sheet-1__PickedSet3
*IMPORT NSET
sht_cen,sht_left_bot
*IMPORT ELSET
sheet-1__PickedSet3,sht_cen
** BOUNDARY CONDITIONS
**
** Name: BC-1 Type: Symmetry/Antisymmetry/Encastre
*Boundary
sht_left_bot, ENCASTRE
** Name: BC-2 Type: Symmetry/Antisymmetry/Encastre
*Boundary
sht_cen, XSYMM
*RESTART,WRITE,FREQ=10
**
*STEP,NLGEOM,INC=50
*STATIC
 0.1,1.
**
**
** OUTPUT REQUESTS
** FIELD OUTPUT: F-Output-1
**
*Output, field, variable=PRESELECT
**
** HISTORY OUTPUT: H-Output-1
**
*Output, history, FREQ=99
*ENERGY OUTPUT, VAR=ALL
*End Step
```

APPENDIX C

MATLAB PROGRAM FOR OBTAINING

CURVE FITTING PARAMETERS

```
%This program is written by Mayuresh M Dhaigude
function nheq1=ANVIL()
% Input Data
thk=input('Enter sheet thickness in mm :  ');
R1=input('Enter first indenter radius in mm :  ');
L1=input('Enter first load in kg :  ');
h1=input('Enter first depth of indentation in mm :  ');

R2=input('Enter second indenter radius in mm :  ');
L2=input('Enter second load in kg :  ');
h2=input('Enter second depth of indentation in mm :  ');

R3=input('Enter third indenter radius in mm :  ');
L3=input('Enter third load in kg :  ');
h3=input('Enter third depth of indentation in mm :  ');

NMAX=100000;
nh1=h1/R1;              nh2=h2/R2;              nh3=h3/R3;
nL1=L1*9.81/(4*R1*R1);  nL2=L2*9.81/(4*R2*R2);  nL3=L3*9.81/(4*R3*R3);
nthk1=thk/R1;           nthk2=thk/R2;           nthk3=thk/R3;
pene1=h1/thk;           pene2=h2/thk;           pene3=h3/thk;
LIM=0.8;

if (pene1>=LIM|pene2>=LIM|pene3>=LIM)

fprintf('\n**************************************************************
*************************************\n');
   fprintf('     INVALID!! Depth of indentation has exceeded the limit !! ');

fprintf('\n**************************************************************
*************************************\n\n');

else
```

```
fprintf('\n**********************************************************************
**************************************\n');
fprintf('     Program for obtainting equivalent depth of indentation without anvil effect ');
fprintf('\n**********************************************************************
**************************************\n\n');

  b=0.00;

for N=1:NMAX


   NUME=(nh1-nh2)*(nthk1-(b*nL1))*(((nthk3-(b*nL3)))-((nthk2-(b*nL2))));
   DENO=((((nthk2-(b*nL2)))-((nthk1-(b*nL1))))*(nthk3-(b*nL3)));
   %chk=(NUME)/(DENO);
   %display(chk);
   S=(nh2-nh3)-((NUME)/(DENO));
      if S>=0.00000
          break;
       else
          b=b+0.0000001;

       end
end

a=((nh2-nh3)*(nthk2-(b*nL2))*(nthk3-(b*nL3)))/(((nthk3-(b*nL3)))-((nthk2-
(b*nL2))));


fprintf('\n**********************************************************************
**************************************\n');
fprintf('     Normalized depth of indentation without anvil effect (heq / R) =
%3.8f',nheq1);
fprintf('\n**********************************************************************
**************************************\n');
fprintf('\n   Curve Fitting parameters:\n\n');
fprintf('     First coefficient (for numerator)= %3.8f, \n     Second coefficient (for
denominator)= %3.12f\n',a,b);
fprintf('\n**********************************************************************
**************************************\n\n');

end
```

VITA

Name:	Mayuresh Mukund Dhaigude
Address:	17/71, ‘Audumbar’, Manmohan society, Karvenagar, Pune, India 411052.
Email address:	dmayureshd@yahoo.com
Education:	M.S. Mechanical Engineering, Texas A&M University, August 2006
	B.Eng., Mechanical Engineering, University of Pune, India July 2002